2006

Long-Term ENSO-Related Winter Rainfall Predictions over the Southeast U.S. Using the FSU Global Spectral Model

Dawn C. Petraitis

THE FLORIDA STATE UNIVERSITY

COLLEGE OF ARTS AND SCIENCES

LONG-TERM ENSO-RELATED WINTER RAINFALL PREDICTIONS OVER THE SOUTHEAST U.S. USING THE FSU GLOBAL SPECTRAL MODEL

By

DAWN C. PETRAITIS

A Thesis submitted to the
Department of Meteorology
in partial fulfillment of the
requirements for the degree of
Master of Science

Degree Awarded:
Summer Semester, 2006

The members of the Committee approve the thesis of Dawn C. Petraitis defended on April 21, 2006.

_____
James J. O'Brien
Professor Directing Thesis

_____
Carol Anne Clayson
Committee Member

_____
Fei-Fei Jin
Committee Member

The Office of Graduate Studies has verified and approved the above named committee members.

To my late grandmother, Helen Lasich, who always supported my dreams. She knew about this step in my life, but never got to see me fly.

ACKNOWLEDGEMENTS

The funding for this research came from the NOAA Office of Global Programs as an Applied Research Center to Dr. James J. O'Brien.

NCEP Reanalysis data was provided by the NOAA-CIRES Climate Diagnostics Center, Boulder, Colorado, USA, from their Web site at http://www.cdc.noaa.gov/.

Several people have offered assistance on this project along the way. First, I would like to thank my major professor, Dr. O'Brien, for offering me the opportunity earn my Masters degree. I would also like to thank my committee members, Carol Anne Clayson and Fei-Fei Jin, for their valuable input. Many thanks go to Tim LaRow for the unending assistance on so many things while working on this project. Thanks also to D. W. Shin and Y. K. Lim for their assistance with the observational datasets. I would also like to thank Melissa Griffin for her assistance with the on-going statistical testing program issues.

Finally, I would like to thank all the people who have supported me through this journey. Thank you to my parents, Donald and Deborah, for always pushing me to do my personal best in everything, and my sister, Diane, for always being there for me no matter what. Thanks also to my best friend, Jessica Davis, for being there throughout the years and always believing in me. Finally, I would like to thank my best friend/boyfriend, Kevin Martin, for totally understanding all the stress that went into the preparation of this paper and for listening to all my never-ending ideas.

TABLE OF CONTENTS

LIST OF TABLES

LIST OF FIGURES

ABSTRACT

Rainfall patterns over the Southeast U.S. have been found to be connected to the El Niño-Southern Oscillation (ENSO). Warm ENSO events cause positive precipitation anomalies and cold ENSO events cause negative precipitation anomalies. With this level of connection, models can be used to test the predictability of ENSO events. Using the Florida State University Global Spectral Model (FSUGSM), model data over a 50-year period will be evaluated for its similarity to observations.

The FSUGSM is a global spectral model with a T63 horizontal resolution (approximately 1.875°) and 17 unevenly spaced vertical levels. Details of this model can be found in Cocke and LaRow (2000). The experiment utilizes two runs using the Naval Research Laboratory (NRL) RAS convection scheme and two runs using the National Centers for Environmental Prediction (NCEP) SAS convection scheme to comprise the ensemble. The simulation was done for 50 years, from 1950 to 1999. Reynolds and Smith monthly mean sea surface temperatures (SSTs) from 1950-1999 provide the lower boundary condition. Atmospheric and land conditions from January 1, 1987 and January 1, 1995 were used as the initial starting conditions. The observational precipitation data being used as the basis for comparison is a gridded global dataset from Willmott and Matsuura (2005).

Phase precipitation differences show higher precipitation amounts for El Niño than La Niña in all model runs. Temporal correlations between model runs and the observations show southern and eastern areas with the highest correlation values during an ENSO event. Skill scores validate the findings of the model/observation correlations, with southern and eastern areas showing scores close to zero. Temporal correlations between tropical Pacific SSTs and Southeast precipitation further confirm the model's ability to predict ENSO precipitation patterns over the Southeast U.S. The inconsistency in the SST/precipitation correlations between the models can be attributed to differences in the 200-mb jet stream and 500-mb height anomalies. Slight differences in position and strength for both variables affect the teleconnection between tropical Pacific SSTs and Southeast.

CHAPTER 1

INTRODUCTION

The prediction of El Niño-Southern Oscillation (ENSO) teleconnection patterns by global models is important for regional climate simulations. These regional climate simulations have important applications for seasonal weather predictions, such as crop modeling (Shin et al. 2005, Cocke et al. 2006). In order to predict accurately regional climate on a high-resolution grid (Cocke and LaRow 2000, Cocke et. al 2006), the global models, coupled with the regional models, must also have skill in predicting ENSO teleconnections. Failure by the global model to predict accurately ENSO patterns will create errors in the regional simulation in areas where the ENSO signal is known to exist. Thus to improve regional climate simulations, we must evaluate the global model forecasts. The skill of the Florida State University Global Spectral Model is assessed through a comparison of the model to observations using seasonal precipitation.

Statistical links between ENSO and surface parameters have been suggested as early as the 1920s and 1930s (Walker 1924, Walker and Bliss 1932). Only more recently has the validity of these possible links been investigated. Ropelewski and Halpert (1986) separated North America into five different regions and found that the Southeast U.S. (Gulf of Mexico region) and the inter-mountain Southwest U.S. (Great Basin region) had a consistent ENSO-related precipitation signal. Using observational data, they showed that the Southeast U.S. had positive precipitation anomalies from October (0; onset year of an ENSO event) to March (+1; one year after onset of an ENSO event). They theorized that the response over the Southeast U.S. could be an indication of a more direct link to ENSO forcing rather than a teleconnected pattern, such as the Pacific-North American (PNA) pattern. They further stated that this direct link to the ENSO forcing may have accounted for the consistency of the precipitation response over the region.

Ropelewski and Halpert (1987) investigated the “typical” global precipitation patterns associated with ENSO. Also using observational data, they found several regions around the

globe that had consistent precipitation patterns directly related to ENSO. They identified two regions in North America that were found to have coherent ENSO-related precipitation, as in their previous study. They further concluded that mid-latitude precipitation and ENSO are linked only over the Indian subcontinent and parts of North America in the Northern Hemisphere while the two parameters are linked for all the major Southern Hemisphere land masses.

The emphasis of this research is to study the Southeast precipitation patterns that result from the teleconnections, not the teleconnections themselves. However, it is important to understand the means by which these patterns develop. One teleconnection between ENSO and the Southeast U.S. is the PNA pattern (Leathers et al. 1991, Livezey et al. 1997). However, the PNA pattern can be excited by the propagation of a Rossby wave (Horel and Wallace 1981) or the Asian jet stream (Lau and Boyle 1987) in addition to ENSO. Several studies have examined the various effects of the PNA pattern on North American climate. Leathers et al. (1991) found that the PNA index, a measure of the strength and phase of the PNA pattern, was correlated with monthly temperature and, to a lesser degree, monthly precipitation in numerous U.S. climate regions, with the highest correlations located in the Southeast and Northwest U.S. They concluded that the PNA teleconnection was an important factor in climate variation over certain regions of the U.S. during the months when the PNA pattern is a major mode of atmospheric variability in the Northern Hemisphere. Leathers and Palecki (1992) used a time series of monthly values of the PNA index to explain the results from the Leathers et al. (1991) study. They found that the explained variance of the PNA index was relatively high in the winter months, with both tropical SSTs and proxy measurements of the strength and position of the East Asian jet being important members of the PNA index specification equations. During a warm ENSO event, the PNA index values result in a positive tendency, while index values tend to be negative during a cold ENSO event (Yarnal and Diaz 1986). Livezey et al. (1997) focused on the PNA region responses to considerable SST anomalies in the central equatorial Pacific Ocean. They note that this specific region of the Pacific is where the strong anomalies have occurred during strong ENSO events. For precipitation, almost year-round teleconnections were found for positive SST anomalies but could not be identified in late summer (Livezey et al. 1997). Negative SST anomalies and precipitation combined to show year-round teleconnections also (Livezey et al. 1997). In addition, teleconnections for precipitation from pre-winter to pre-spring were highly linear between positive and negative SST anomalies (Livezey et al. 1997).

Deser et al. (2004) used an index based on sea level pressure, called the North Pacific Index (NPI), as a measure of the strength of the PNA pattern rather than a mid-troposphere based index such as the PNA index. They stated that negative NPI values correspond to a stronger Aleutian low pressure system with strengthened westerly winds across the central North Pacific and intensified southerly (northerly) winds over the eastern (western) North Pacific; positive NPI values are found with the opposite conditions. This study was specifically focused on interdecadal climate variation, where NPI values were positive or negative for long periods of time (~20-30 years). Their analysis supported past results that found major shifts in the winter NPI were associated with climate fluctuations over the tropical Indo-Pacific region. It is important to note that the time period used for the research presented here (1950-1999) contains a major climate shift.

Another important feature to note is the delayed atmospheric response to the warm phase of ENSO. Hoerling and Kumar (2000) showed that the seasonal predictability of the midlatitudes associated with tropical forcing is encapsulated almost exclusively within a single response pattern. They stated that the tropical forcing during ENSO is not very different between events. They found that the midlatitude response changed when rainfall was enhanced in the far eastern equatorial Pacific. This atmospheric change included a downstream shift of the North American anticyclone response relative to weaker warm events, in addition to an increase in the size of the North Pacific cyclone response. These findings infer a delayed response of the atmosphere to tropical SST forcing. Kumar and Hoerling (2003) found a 1-3 month atmospheric lag between the Niño-3.4 region (5°N-5°S, 120°-170°W) SST index and observed zonal mean tropical 200-mb heights. They summarized that the one season lag in the atmospheric response is linked to time evolution of tropical rainfall during ENSO. Since the tropical rainfall lags the Niño-3.4 index by one season, the one season lag of the atmosphere relative to the Niño-3.4 SST anomalies occurs (Kumar and Hoerling 2003). This result means that while the Niño-3.4 SST anomalies peak in early winter, the zonal mean rainfall anomalies peak in late winter (Kumar and Hoerling 2003). The one season lag by the atmosphere can then be applied to this research, by focusing on wintertime precipitation.

Numerous modeling studies have also been done to aid in the understanding of ENSO teleconnections, both in the short-term and long-term. Quan et al. (2004) focused on short-term seasonal predictions using a spectral model forced by SSTs. They attempted to find mechanisms

that determined the seasonality of SST-forced atmospheric prediction by focusing on the SST forcing and the atmospheric external variability over the tropical Pacific. LaRow and Krishnamurti (1998) used a coupled ocean-atmosphere global model to study seasonal ENSO predictions from 1986 to 1988. The ocean model was used in the study as a substitute for observed SSTs as a boundary condition. Cocke and LaRow (2000) embedded a regional spectral model within the coupled ocean-atmosphere global model to study ENSO patterns during the winters of 1987 and 1988. They concluded that the coupled global model reproduced the large-scale ENSO precipitation patterns, with the regional model being very consistent with the global model but with more detail around coastlines and mountains. Kao et al. (1996) found that the National Center for Atmospheric Research (NCAR) Community Climate Model Version 2 (CCM2) produced realistic features of the ENSO-scale time evolution of simulated precipitation over the central equatorial Pacific. This corresponds well to the regional model results presented by Cocke and LaRow (2000).

A study by Shin et al. (2005) found that the inclusion of the NCAR Community Land Model Version 2 (CLM2) as the land parameterization in the FSUGSM improved simulations of surface temperature and precipitation when compared to the original, simplified FSU land scheme. The use of the NCAR CLM2 appeared to have more of an effect than the choice of convective scheme (four used in the study) on precipitation amounts. However, the authors theorized that the convective scheme might play a more important role than the land scheme for higher threshold precipitation values.

Due to the predictability of ENSO patterns over the Southeast U.S., our research will focus on precipitation over this region. Two distinct configurations develop over the region during winter in response to the tropical Pacific Ocean. During a warm ENSO event (El Niño), warmer SSTs in the eastern tropical Pacific Ocean lead to above normal precipitation in the coastal areas of the Southeast. During a cold ENSO event (La Niña), cooler SSTs in the eastern tropical Pacific Ocean lead to below normal precipitation in the coastal areas of the Southeast. When neither a cold nor warm event occurs, the phase is considered to be neutral, which is incorrectly associated with near-normal climate patterns. The neutral phase actually corresponds to a more variable climate which encompasses a wide range of possible outcomes. The model output will be assessed with the understanding that the neutral phase is highly variable.

Since this research encompasses multiple model runs, a simplified application of the DEMETER (Development of a European Multimodel Ensemble System for Seasonal to Interannual Prediction) project can prove useful, where our ensemble consists of two different models. Palmer et al. (2004) developed a multimodel ensemble system that included seven European global coupled ocean-atmosphere models. They showed that the multimodel ensemble performed better than the single-model ensemble for all ensemble sizes. They found that the multimodel ensemble provided a better sampling of forecast uncertainty given that it contained the verification more often than a single-model ensemble. Their results indicated that the multimodel ensemble is a viable approach to the model uncertainty problem in seasonal-to-interannual prediction.

The goal of this research is to assess the skill of the FSUGSM with respect to observations in predicting seasonal precipitation patterns over the Southeast U.S. In order to evaluate the model, a comparison study using observational data over the same domain will be performed. The initial objective is to obtain similar results as Shin et al. (2005) and Cocke et al. (2006) but using a longer time period, thus giving some insight into the skill of the model in producing long-term forecasts using observed SSTs.

The paper is organized as follows. Section 2 describes the data and the methodology of the study, including background on the FSUGSM. The results are presented in Section 3, with a discussion of the findings in Section 4. Future work and conclusions are given in Section 5.

CHAPTER 2

DATA AND METHODOLOGY

The model used in this study consists of the FSU Global Spectral Model (FSUGSM) coupled to the National Center for Atmospheric Research Community Land Model 2 (NCAR CLM2). The FSUGSM is a spectral model run with a horizontal resolution of T63 (approximately 1.875°) and a vertical resolution of 17 unevenly spaced sigma levels. Details of this model can be found in Cocke and LaRow (2000). For this research, four model runs were performed with two runs using the Naval Research Laboratory (NRL) RAS convection scheme, and two runs using the National Centers for Environmental Prediction (NCEP) SAS convection scheme. Differences between the two convection schemes lie in how cumulus cloud ensemble is calculated and converted into precipitation, which will affect the amount of rainfall over the model domain. The model was run for a period of 50 years, using Reynolds and Smith monthly mean SSTs from 1950-1999 as the lower boundary condition. Model runs were either initialized with 12 UTC 1 January 1987 or 1 January 1995 initial atmospheric and land conditions as boundary conditions thus yielding an ensemble size of four members. Each model experiment took approximately 22 days and 4184 hours of CPU time to run on the IBM supercomputer using 16 CPUs.

The observational precipitation data, used as the basis for comparison to the FSUGSM, is a gridded global dataset from Willmott and Matsuura (2005). This dataset is based on monthly station averages of precipitation interpolated to a 0.5° by 0.5° latitude/longitude grid. The above grid was then expanded to the same dimensions as the model grid using a bilinear interpolation routine for arbitrarily specified coordinates (i.e. a spectral grid rather than a linear grid).

Each year of the 49-year period common to both the model and observations was categorized according to the Japan Meteorological Agency (JMA) ENSO Index to assess the impact of ENSO over the Southeast U.S. The JMA Index uses the monthly SST anomaly in the region 4°S to 4°N, and from 150°W to 90°W (JMA 1991). The index is calculated as a 5-month

running mean of SST anomalies over the specified region (JMA 1991). The ENSO phase for a specific year is defined as follows: the phase is categorized as El Niño if the JMA Index is above 0.5°C for six consecutive months; conversely, the phase is categorized as La Niña if the index is below -0.5°C; the phase is Neutral in all other cases (JMA 1991). Figure 1 shows the time series of monthly SST anomalies from 1950 to 1999 over the JMA area. The ENSO year for the JMA Index begins in October; for example, the El Niño year of 1997 began in October 1997 and continued until September 1998. Applying the JMA Index for the 49-year period

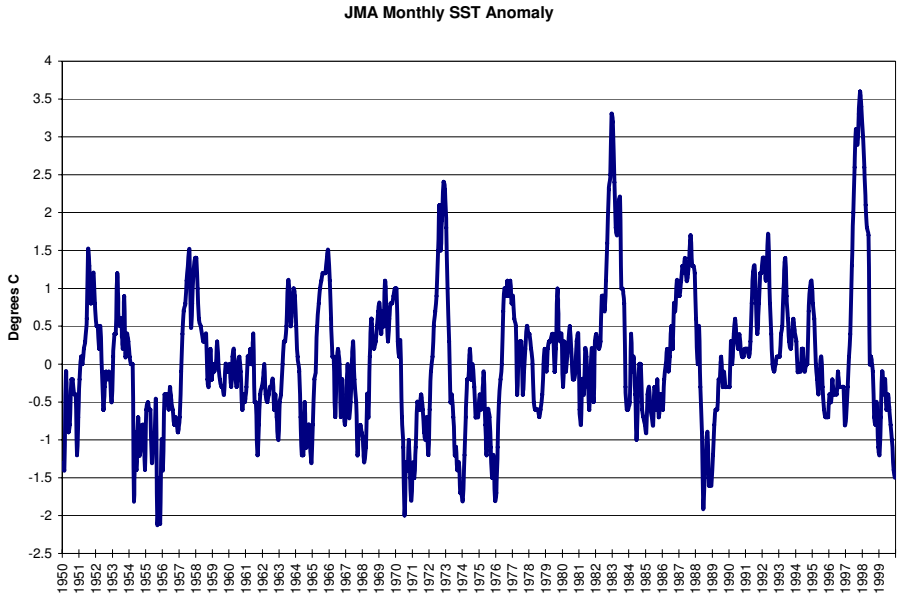

Figure 1: Monthly JMA SST anomalies for 1950-1999.

beginning in 1950 and ending in 1999, we obtain 12 El Niño years, 12 La Niña years, and 25 Neutral years. Table 1 shows the phase classification of each year in the 49-year period. From this classification, phase composites are computed. The phase composites are the average of all seasons for each specific ENSO phase.

Two types of correlation coefficients are calculated using the above data. The first type of correlation is a spatial correlation. This form of correlation indicates the similarity of one map compared to another map; in this case, the similarity of a model compared to the observations. Further, two sets of spatial correlations are calculated. The first correlation coefficient uses the entire time period average to develop an overall view of the forecasting skill of the model. The second correlation coefficient breaks the data down into ENSO phase, which yields insight into

Table 1: JMA ENSO phase classification for the years 1950-1999.

Cold	Neutral	Warm
1954	1950	1951
1955	1952	1957
1956	1953	1963
1964	1958-1962	1965
1967	1966	1969
1970	1968	1972
1971	1977-1981	1976
1973	1983	1982
1974	1984	1986
1975	1985	1987
1988	1989	1991
1998	1990	1997
	1992-1996	

the ability of the model to forecast each ENSO phase. Spatial correlations based on the total DJF precipitation for both climatology (seasonal average) and ENSO phase are calculated.

The second type of correlation coefficients, temporal correlations, is subsequently calculated. These correlations are calculated at each grid point over a specified length of time. The ability of the model to develop different spatial patterns is shown through these correlations. The first set of temporal correlations is between the observational precipitation fields and the model precipitation fields. These correlations are calculated for the seasonal average, ENSO signal, and neutral phase.

A lag correlation between the JMA SSTs and the precipitation over the Southeast is also calculated. This calculation shows the amount of time (in months) between the peak SSTs over the tropical Pacific and the peak precipitation over the Southeast. The equation used to calculate the lag correlation is

$$r(d) = \frac{\sum_{i=1}^{n-d}[(x_i - \bar{x})(y_{i-d} - \bar{y})]}{\sqrt{\sum_{i=1}^{n-d}(x_i - \bar{x})^2}\sqrt{\sum_{i=d+1}^{n-d}(y_{i-d} - \bar{y})^2}}, \quad (1)$$

where x is the JMA box-averaged SSTs, y is the area-averaged precipitation over the Southeast, and d is the number of lags in months. This equation produces correlation coefficients for multiple lags by changing d.

A different set of temporal correlation is also calculated. This specific correlation is a measure of the teleconnection of the tropical Pacific to the Southeast. The correlation value is calculated using the area-averaged SST over the JMA region and the Southeast precipitation. Seasonal averages are used in the calculation of the correlation. Correlations are calculated for the entire 49-year period, the ENSO signal in general, and the neutral phase.

Model bias illustrates the tendencies of the model to either over- or under-predict the amount of precipitation over a given area. The bias is calculated simply by subtracting the observations from each of the four models. A bias calculation is done for the seasonal averages and the ENSO phase composites.

Another way of testing the skill of the model overall is to combine each of the four model runs into a model ensemble. The model ensemble gives each individual model run equal weight; therefore, it is a straight average of the four model runs. As with each ensemble member, bias and spatial correlations are calculated.

Variance of the model and observational precipitation fields assists in evaluating the skill of the model. It also gives an insight into the variability within each dataset. Variance is calculated using the equation

$$s^2 = \frac{1}{n-1}\sum_{i=1}^{n}(x_i - \bar{x})^2 , \qquad (2)$$

where x_i is the precipitation for a given season, $\bar{x}$ is the mean precipitation over time, and n is the number of time steps in the dataset. The variance is calculated for the 49-year period, the ENSO signal, and the neutral phase.

Skill scores are another method of comparing the model precipitation fields to the observation fields. They complement the model/observation correlation coefficients. The particular skill score calculated here incorporates the mean-squared error (MSE). The MSE equation equals

$$MSE = \frac{1}{n}\sum_{k=1}^{n}(y_k - o_k)^2 , \qquad (3)$$

where y_k is the model precipitation, o_k is the observational precipitation, and n is the number of time steps in the dataset. A similar equation is used to calculate the MSE for climatology, which is the observational dataset here. A substitution of $\bar{o}$ for y_k in Equation (3) gives the climatology

MSE, which is needed for the calculation of the skill score. Using the MSE terms from above, the skill score equation is

$$SS_{c\lim} = \frac{MSE - MSE_{c\lim}}{0 - MSE_{c\lim}} = 1 - \frac{MSE}{MSE_{c\lim}}. \quad (4)$$

The zero in the denominator of the expanded equation is the MSE for a perfect forecast. The upper bound of the skill score is one, which is a perfect score. A skill score of zero means there is no improvement over the reference forecast of climatology.

Other atmospheric variables are analyzed to assess the large scale patterns that influence the climate over the Southeast. NCEP reanalysis data is used here as the basis for comparison to the model. Wind data is utilized to study jet stream patterns over the Southeast. The model outputs u and v components for various vertical levels. The 850-mb level and the 200-mb level are the only levels studied. These levels are critical for precipitation formation over the Southeast. The 850-mb level supplies low level moisture to the region. The 200-mb level acts as the steering current in addition to a primary teleconnection to the tropical Pacific. This level can also supply moisture to the region, albeit a more distant source of moisture. The wind data will be used to create jet stream patterns for each ENSO phase in each model run. Additional data used to understand the atmospheric flow over the Southeast are the 500-mb height anomalies over the PNA region. The 500-mb height anomalies yield an insight into the mid-level flow, which also acts as a primary teleconnection between the tropical Pacific and the Southeast.

CHAPTER 3

RESULTS

Precipitation over the Southeast has been found to be highly predictable in the boreal winter season (e.g. Ropelewski and Halpert 1986, 1987; Livezey et al. 1997; Cocke and LaRow 2000). Coastal precipitation amounts in the models should be more similar to the observations than inland areas due to the stronger ENSO signal predictability. Seasonal averages using the entire 49-year period are calculated for the observation data, the four model runs, and the model ensemble. Figure 2 shows the spatial patterns of the seasonal averages for each of the six datasets. The four model simulations are similar to each other, with the model ensemble falling somewhere in between the two model extremes. The ensemble eliminates the variability between the individual models. The observation data is different for the western area of the region, specifically over Mississippi and Alabama where precipitation values are higher than predicted by the model runs. However, all four model simulations show central and south Florida drier than areas further inland. The models produced precipitation patterns that are different than the observation pattern. However, the NRL runs show a pattern closer to the observations than the NCEP runs, in both precipitation amounts and spatial distribution.

The precipitation signal for El Niño and La Niña differs over the Southeast. Figure 3 shows the seasonal precipitation difference between El Niño and La Niña composites. This shows the areas where El Niño precipitation is higher than La Niña precipitation, and vice versa. NRL2 shows the wet signal of El Niño over the southern and eastern regions and the dry La Niña signal in the northern and western areas. This model run is similar to the observational pattern shown in Figure 3a. The other three model runs and the ensemble show El Niño greater than La Niña over the northern and western areas of the domain, opposite to what the observations show.

Bias calculations (model minus observations) show areas of over- or under-estimation by the model as compared to the observations. Figure 4 shows the bias in the model ensemble and each of its four members. Precipitation is under-estimated in all simulations in the western and

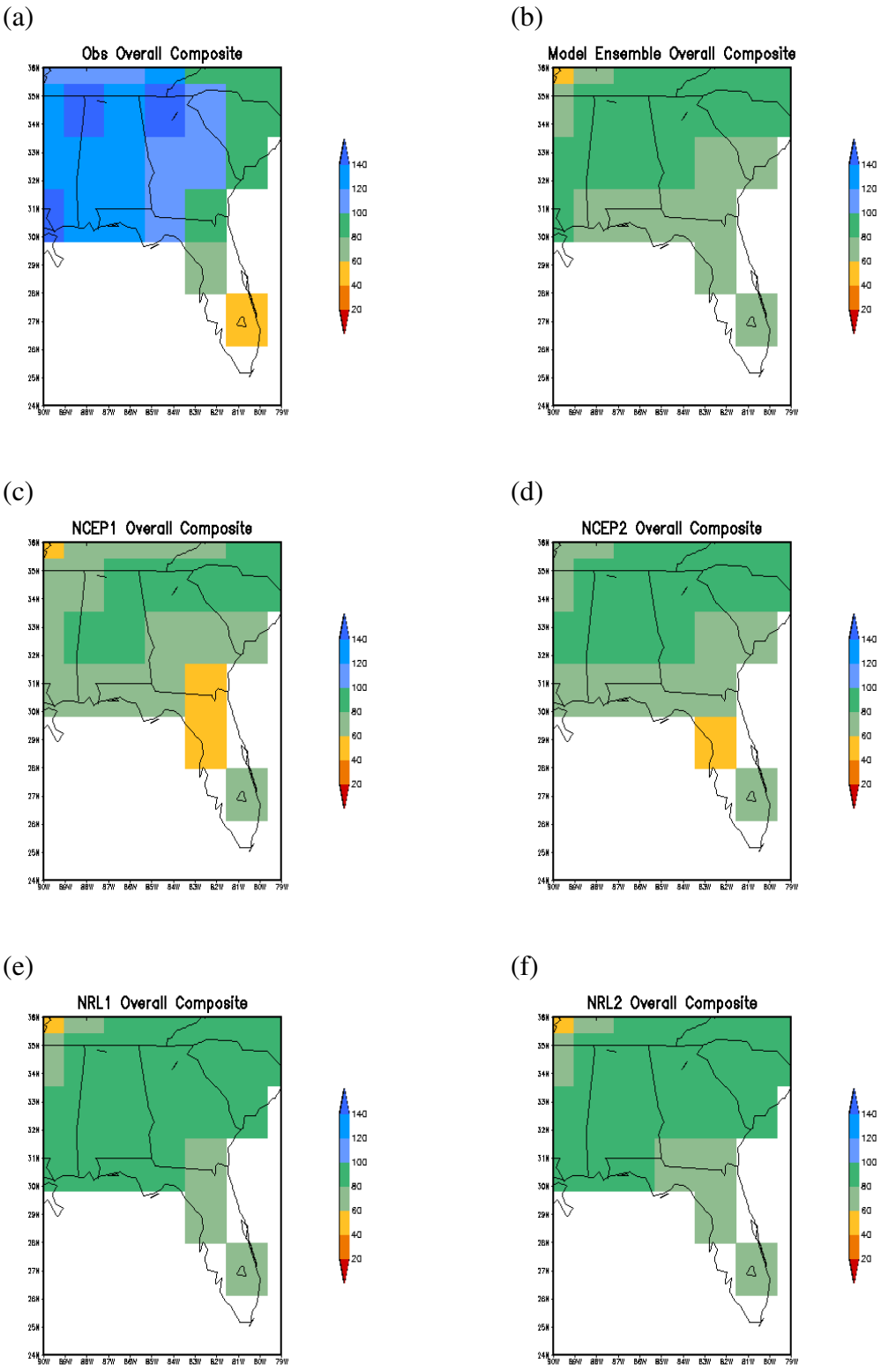

Figure 2: Winter seasonal composites of a) the observations, b) the model ensemble, and c-f) the four individual model runs for 1950-1999. Units are in mm.

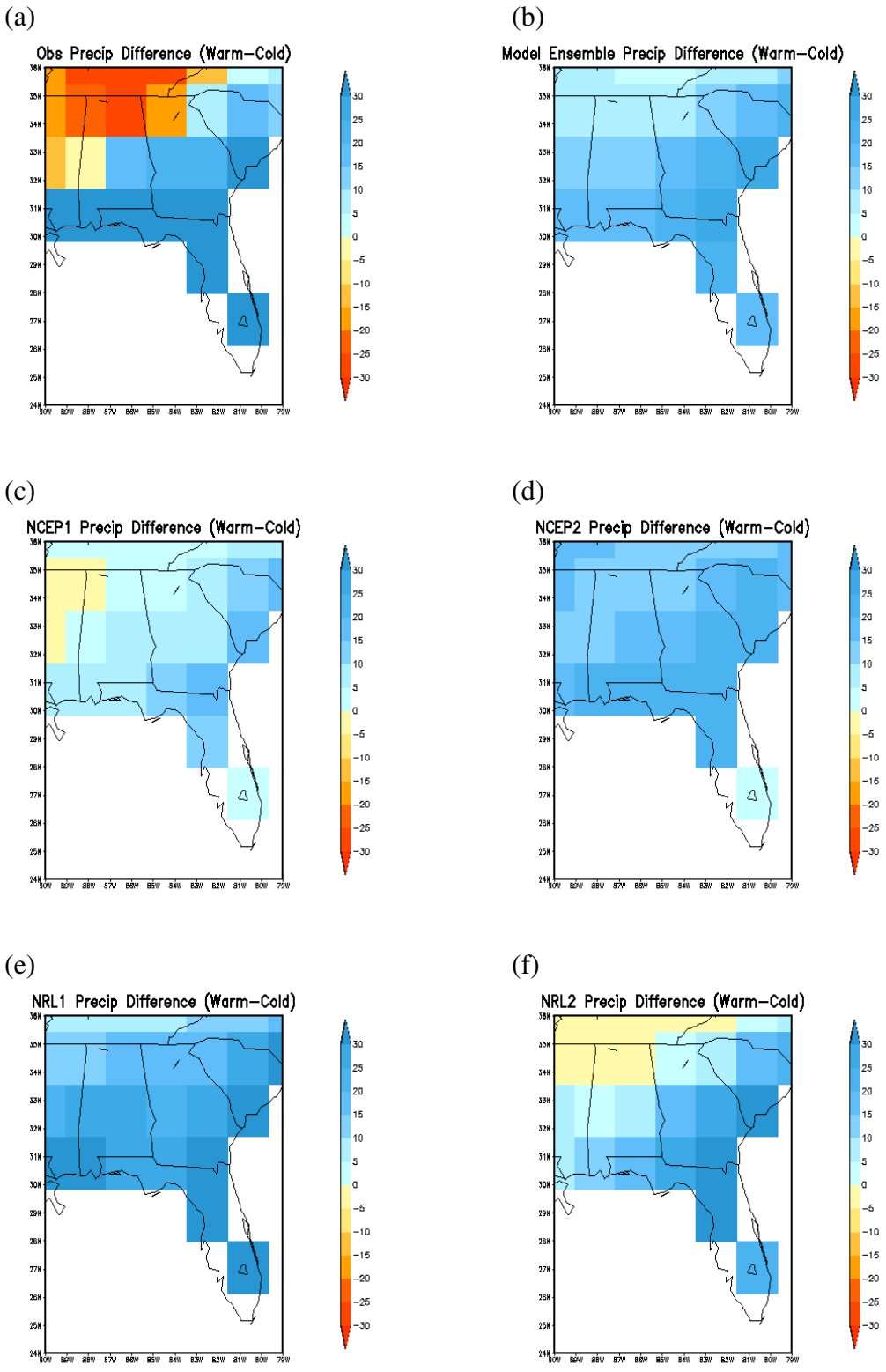

Figure 3: DJF precipitation difference between El Niño (warm) and La Niña (cold) for a) the observations, b) the model ensemble, and c-f) the four models from 1950-1999. Units are in mm.

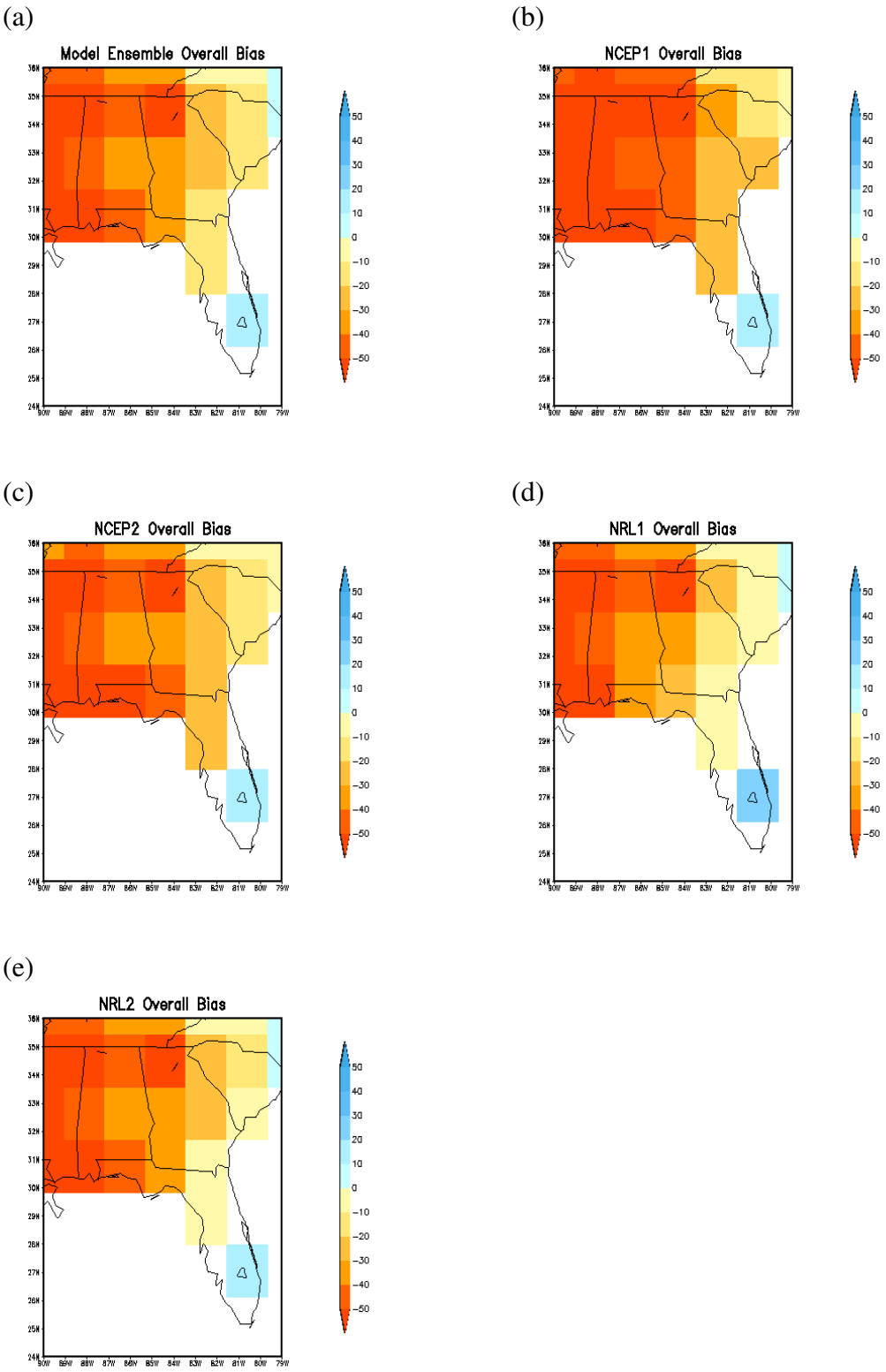

Figure 4: Calculated DJF overall bias (model minus observed) for a) the model ensemble and b-e) the four models. Units are in mm.

central areas of the domain. The simulations also over-predict precipitation in south Florida, with NRL1 over-estimating precipitation by about 10 mm more than the other model runs. Both NRL runs have smaller biases along the Atlantic coast than the NCEP runs. The ensemble bias also shows large under-estimations in western and central areas, with lower under-estimations along the Atlantic coast and slight over-estimations in south Florida. A similar pattern appears over the domain in the ENSO phase composites. Since it is consistent through the model runs and ENSO phases, the bias appears to play only a small role in the similarity between the model and observations.

Spatial correlations are calculated using the boreal winter seasonal averages (composites) for each of the six time series. The four model simulations and the model ensemble are compared to the observations to gauge the ability of the models to forecast spatial patterns. The spatial correlations are calculated using all land grid points in the box from 24°N-36°N and 79°W-90°W. Table 2 shows the correlation values for each of the four simulations and the ensemble. NCEP2 has the highest correlation of all experiments, while NRL1 has the lowest value. The model ensemble lies in the middle of the range of correlation values although still above the median. The ensemble correlation is influenced the most by NCEP2 due to that particular correlation value being much larger than the other 3 models (approximately 0.1 at the least). The critical value for significance at the 95% level is 0.167.

Table 2: Spatial correlation coefficients for each model run and the model ensemble based on overall seasonal averages for all land grid points in the box from 24°N-36°N and 79°W-90°W.

NCEP1	0.595
NCEP2	0.681
NRL1	0.507
NRL2	0.523
Ensemble	0.614

ENSO manifests itself over the Southeast in various ways, with precipitation being one of the key components. The main area of sensitivity, as mentioned before, is the southern and eastern locations due to the positional shift in the jet stream. The model precipitation fields should represent the observations to a certain extent. Generally, precipitation is not simulated by models very well. Therefore, it is unrealistic to expect the model to perfectly match the observations. However, certain areas, such as the coastal areas of the Southeast, should be better

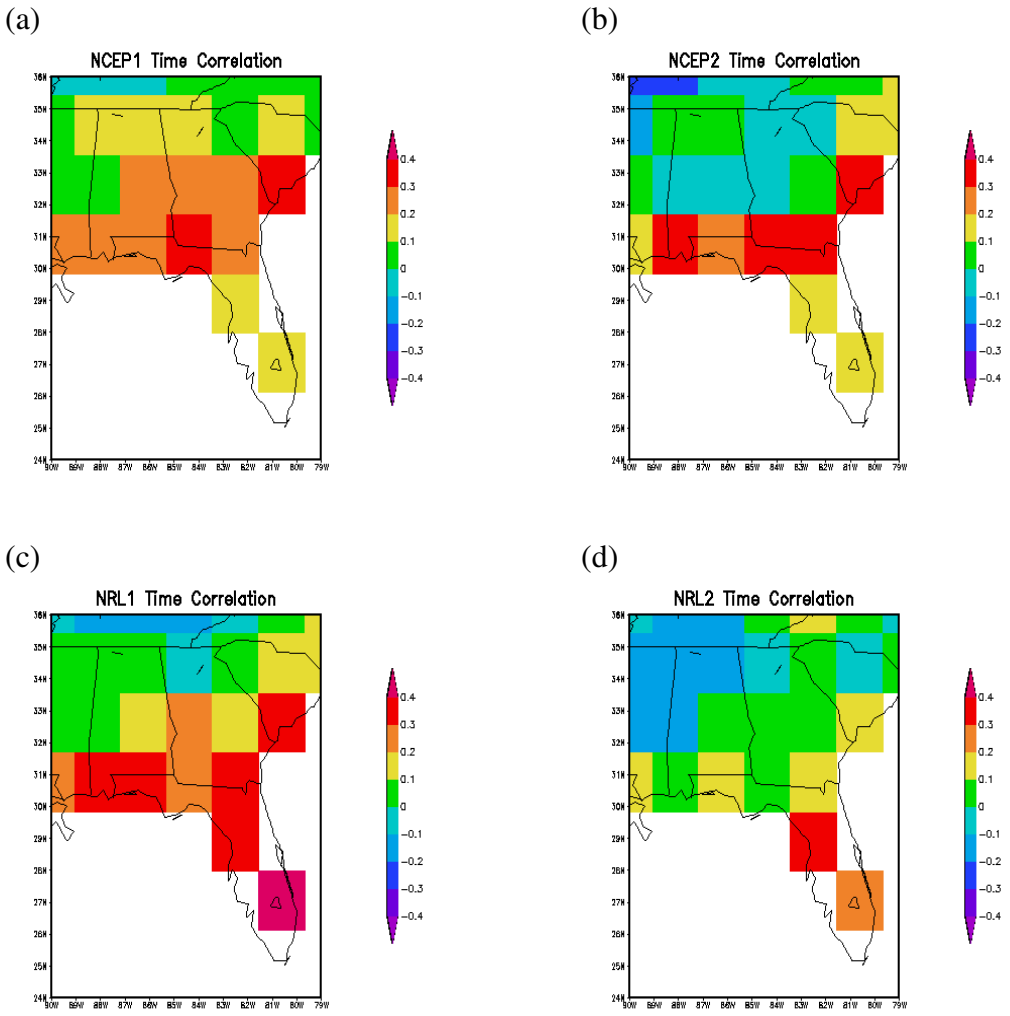

Figure 5: Temporal correlations of the observed precipitation and a-d) the four model runs for 1950-1999.

represented than other regions in the model due to the high sensitivity to ENSO. The stronger the connection between the coastal areas and the tropical Pacific, the higher the model skill will be in predicting precipitation in these areas.

Temporal correlations compare each time step of a dataset to the corresponding time step of another dataset. In this case, each time step of the observations over the 49-year period is compared to the corresponding model output. This particular correlation illustrates differences in the spatial patterns of the model simulations and observations. Figure 5 shows the correlations between the observations and the model runs. The NCEP1 simulation shows a larger area of correlation values greater than 0.2, while the NRL1 simulation shows a smaller area of higher

correlation values restricted to grid boxes that border the coast. Correlations in south Florida are greater than 0.4 in only NRL1, but remain positive for the other three models. NCEP2 and NRL2 show widespread negative correlations (values from -0.1 to -0.2 on average) in the northern and western areas. All four models show more skill in predicting precipitation in the southern and eastern locations. However, high correlation values are not widespread in the southern and eastern areas or consistent between the models. NRL1 shows the highest correlation values in these areas, which corresponds to the highest precipitation amounts in the same locations with respect to the other models. The negative correlations in NCEP2 and NRL2 indicate an inverse relationship between the observations and respective models, but are not negative enough to draw any solid conclusions.

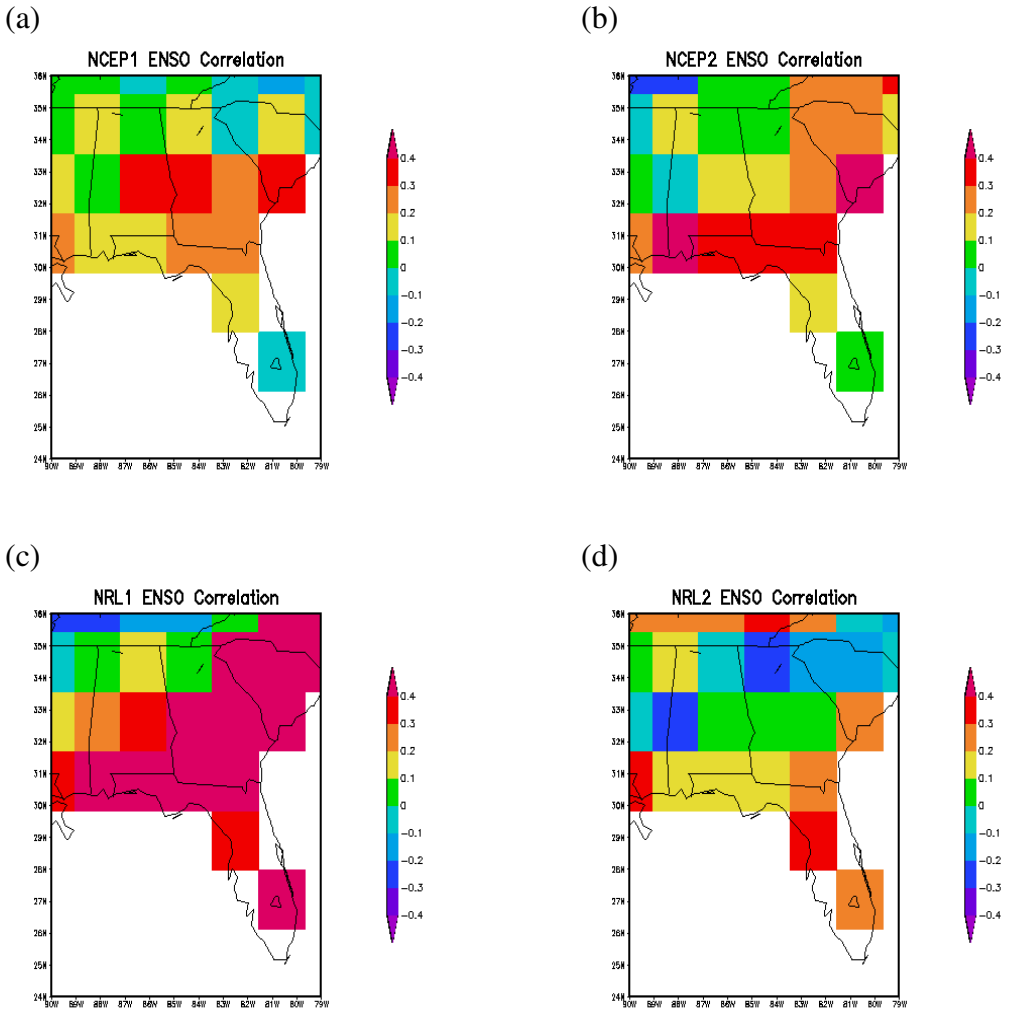

Figure 6: Same as Figure 5, but for the ENSO signal.

The data is the separated into ENSO years and non-ENSO (neutral) years. The ENSO signal correlation, shown in Figure 6, is a combination of the warm and cold years. This particular correlation gives a general idea of how well the models represent the overall ENSO signal. Each of the four individual models shows some degree of similarity to the observations. NRL1 has the highest correlations of any of the model runs in southern and eastern areas. NRL2 shows negative correlation values across northern South Carolina and Georgia. Correlation values of less than -0.2 appear in the extreme northwest corner of the domain in NCEP2 and NRL1. Any negative correlation values indicate an inverse relationship to the observations and thus, ENSO. The only model that has a widespread high connection to the overall ENSO signal

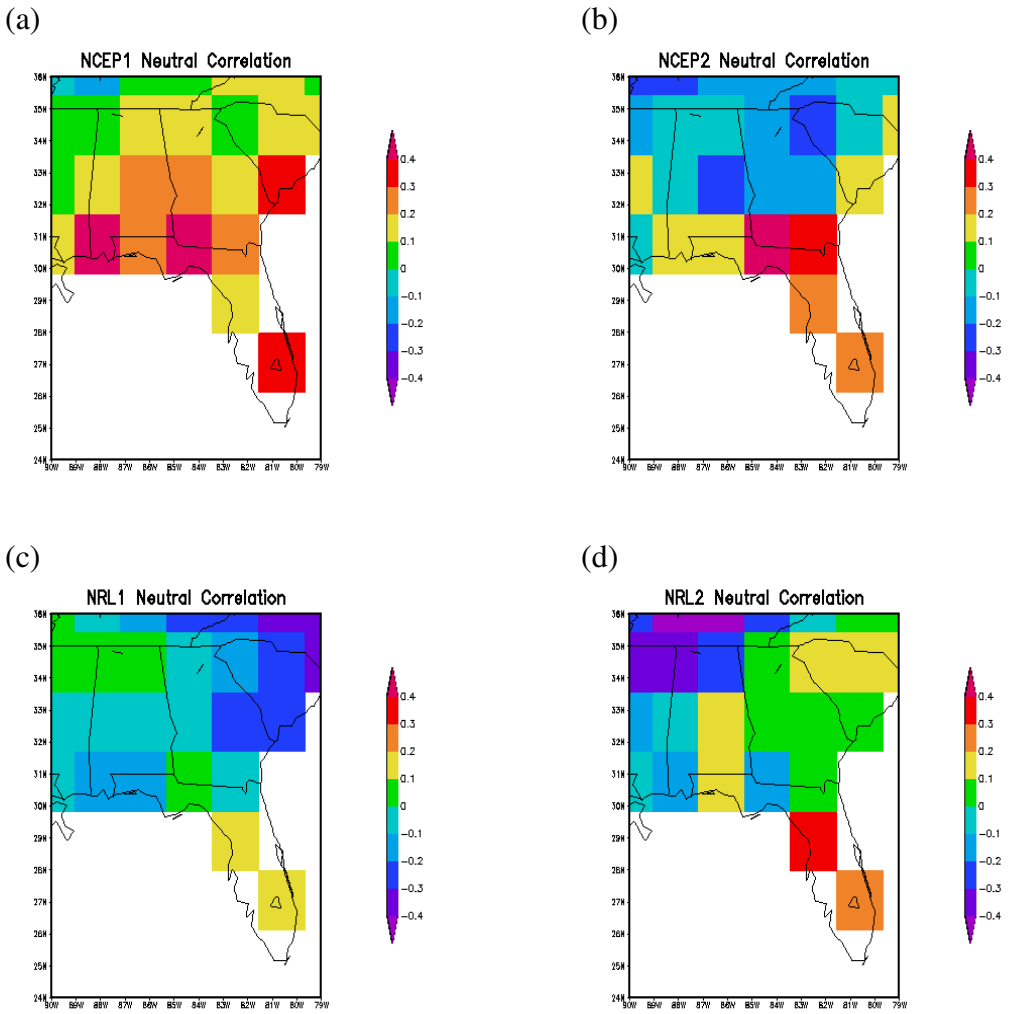

Figure 7: Same as Figure 5, but for neutral.

is NRL1. The general teleconnection between the Southeast and the tropical Pacific may play a role in the similarity of the model fields to the observations, which will be investigated later in the paper.

The neutral phase correlations, as seen in Figure 7, show no major spatial pattern over the domain. NCEP1 and NCEP2 show consistent positive correlations over Florida, but values are not consistent. The NRL runs show correlation values over Florida higher than the rest of the domain. This may hint at some level of sensitivity and predictability to the neutral phase. However, the values over the rest of the domain are marginal at best. The marginal correlation values in the model runs are explained by the variability of the neutral phase, which hampers the predictability of this phase.

Spatial correlations based on phase composites are shown in Table 3. All models yielded their highest correlations for La Niña, except for NCEP2 where the neutral phase has the highest correlation. Correlation values for El Niño are lower than both La Niña and neutral values. This can be interpreted to mean that the models are more able to simulate the axis of maximum precipitation (located southwest to northeast) in La Niña than El Niño. Since La Niña is drier than El Niño, the model precipitation amounts are closer to the observational amounts. However, the model bias remains consistent across phases; therefore, another factor, as yet to be determined, appears to affect these correlation values. The critical value for Table 3 is the same as Table 2.

Table 3: Spatial correlation coefficients of each ENSO phase for each model run and the ensemble using the same domain box as Table 2.

	El Niño	La Niña	Neutral
NCEP1	0.143	0.717	0.646
NCEP2	0.344	0.672	0.747
NRL1	0.272	0.721	0.484
NRL2	-0.232	0.773	0.628
Ensemble	0.186	0.744	0.679

Variance of the precipitation fields shows the difference of each location with respect to an area average. It is a statistic calculated using a time series. These calculations look into the ability of the model to reproduce patterns. Variance for the entire 49-year period, the ENSO signal, and the neutral years is calculated. Figure 8 shows the variance for the observations and

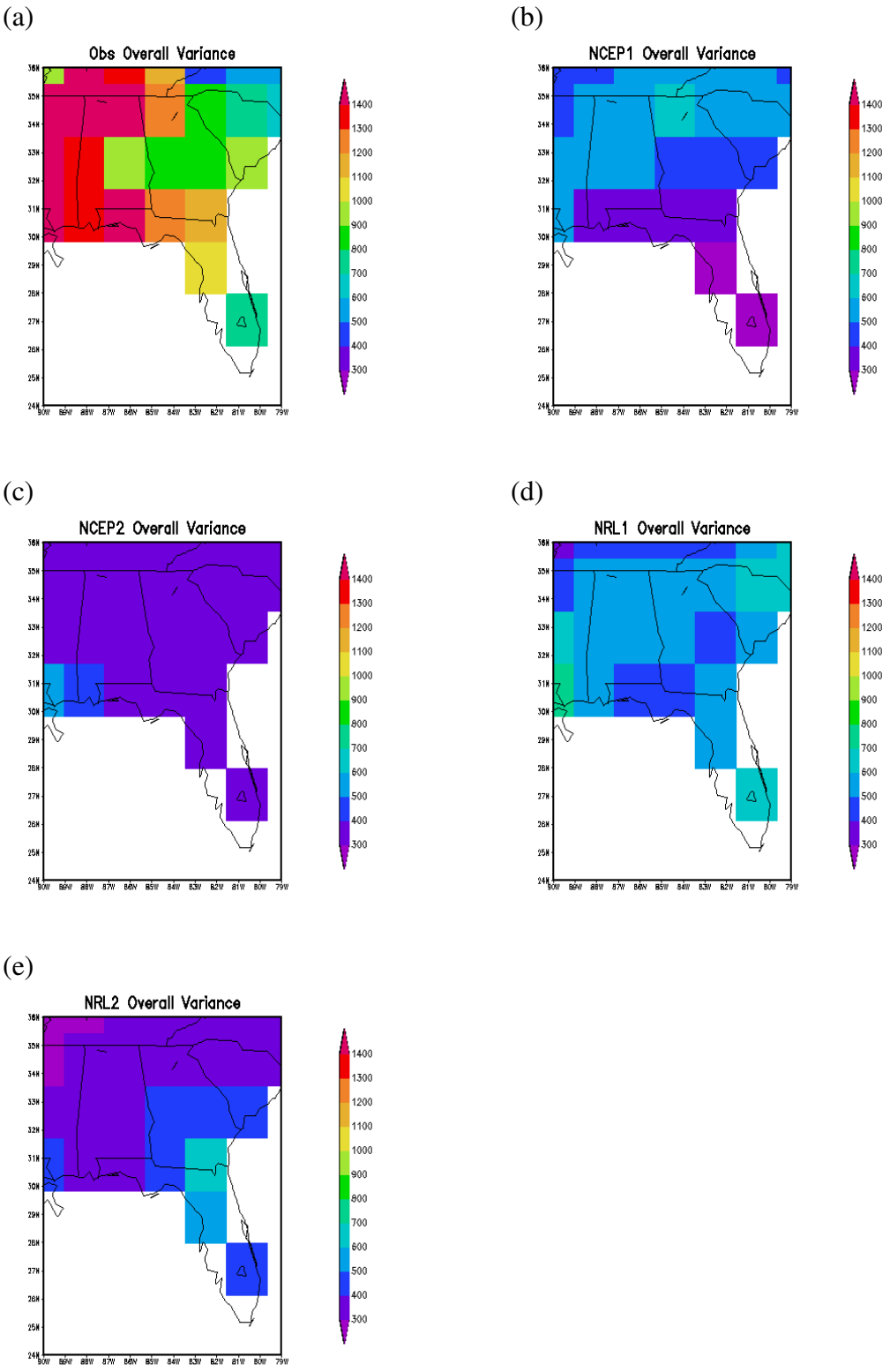

Figure 8: Variance for the 49-year period for a) the observations and b-e) the four model runs. Units are in mm^2.

the four models over the 49-year period. The observational variance is high over the western areas of the domain, with decreasing values moving east. All four models have a lower variance than the observations and do not show the same pattern as the observations. NRL1 has a higher average variance over the whole domain than the other three models, with NCEP1 showing similar variances over the Appalachian Mountains and the foothills. Both NCEP2 and NRL2 show variances lower on the average compared to the other two models. The model variances may be affected by the overall dry bias in the model as well as teleconnection issues.

Variance for the ENSO signal is shown in Figure 9. The highest variance in the observations has shifted from the western areas in the seasonal plots (Figure 8a) to the southern areas for the ENSO signal. The models also show an increase in variance compared to the seasonal plots. Similar to the seasonal variance in Figure 8d, NRL1 shows the highest area-averaged variance of the four models. NCEP2 also shows a similar pattern to the seasonal variance (Figure 8b) with increased values along the Appalachians. NRL2 increases the variance over Florida compared to the seasonal variance (Figure 8e), while NCEP1 shows a decrease over South Carolina and northern Georgia. Again, the model variances may be affected by the dry bias present throughout the model integration.

Neutral variance for the observations and the four model runs is shown in Figure 10. The observations shift the area of highest variance back to the west, similar to the seasonal variance. The model variances also show similar patterns to the seasonal variances in Figure 8, but with decreased values across the domain. NCEP1 shows the highest variances of the four models with the values located along the Appalachians and the foothills, similar to the previous model run results (Figures 8b and 9b). The model runs should show higher variances due to the known variability of the neutral phase, but may be influenced by the dry bias of the model.

Skill scores are another method of comparing two datasets. These will complement the temporal correlations calculated previously. Mean squared error is used in the calculation of these skill scores. A score of zero means there is no improvement over the reference forecast, which is the observational dataset for this case. Figure 11 shows the skill scores calculated using the entire 49-year period. NRL1 shows scores greater than -1 over southern and eastern areas of the domain, while the other three models restrict the same values to only eastern areas. Scores close to zero (greater than -1) can be interpreted to show locations where the model is more similar to the observations than other locations with lower skill scores.

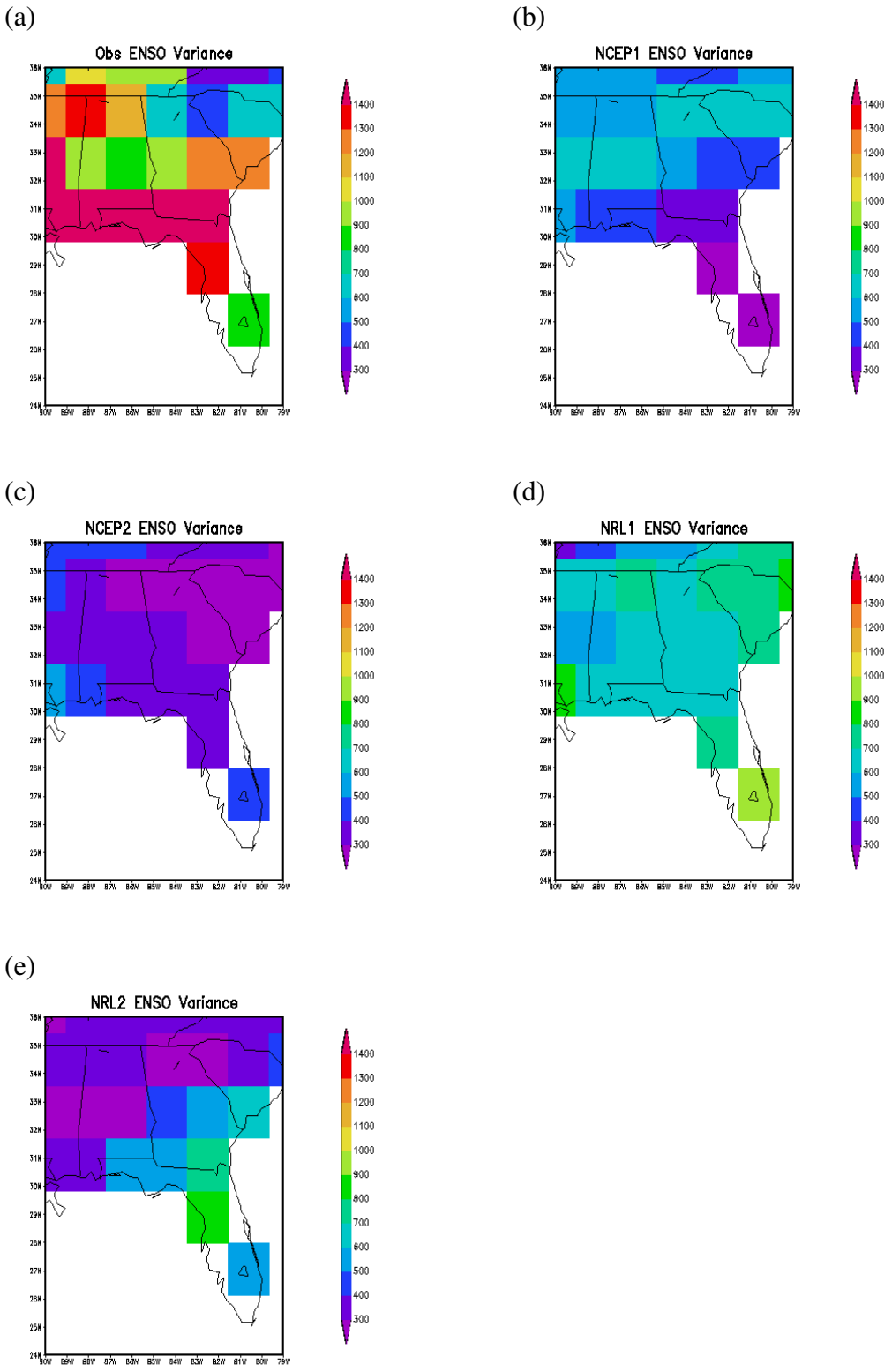

Figure 9: Same as Figure 8, but for the ENSO signal.

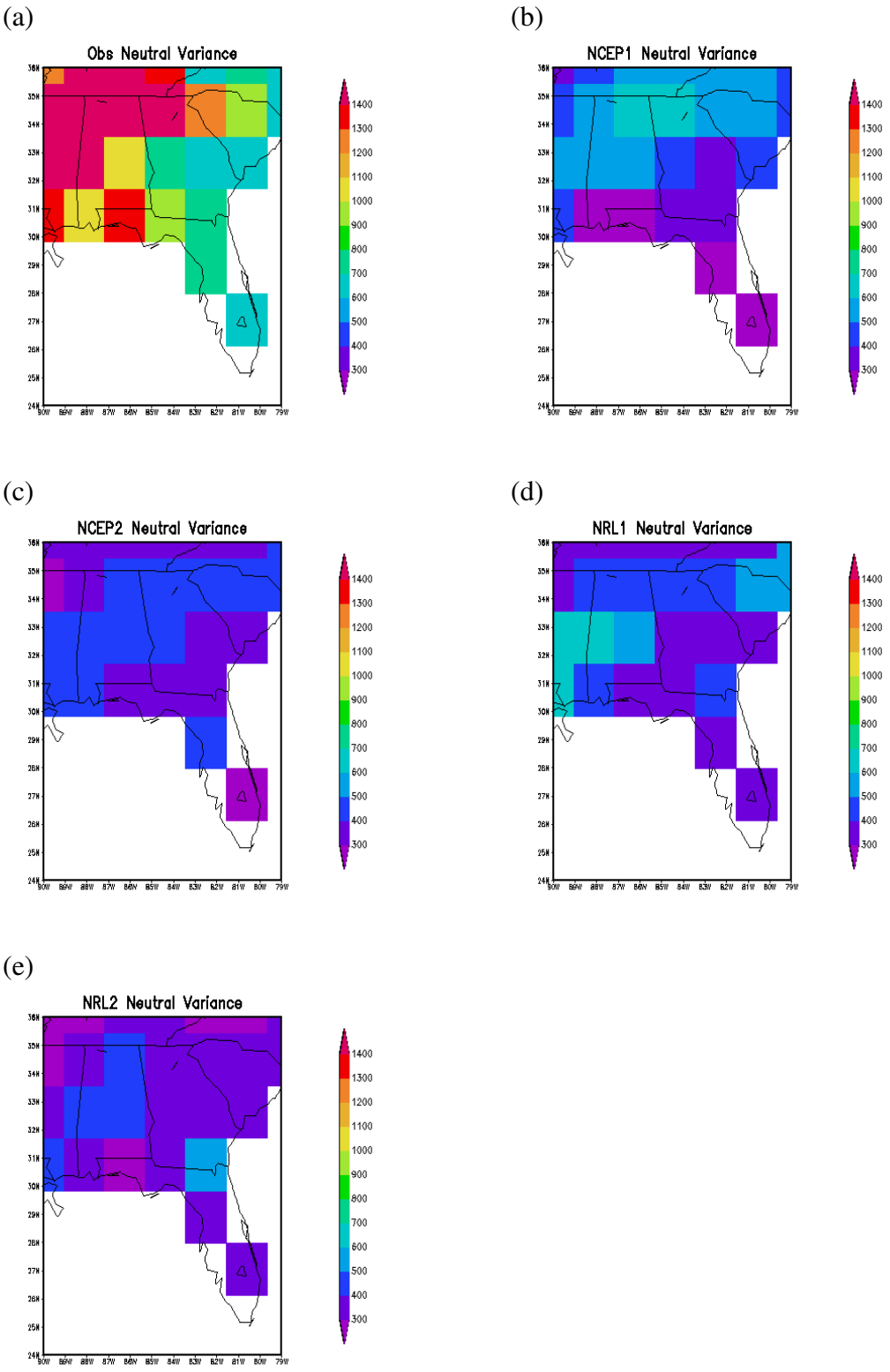

Figure 10: Same as Figure 8, but for the neutral phase.

Figure 12 shows the skill scores for the ENSO seasons only. These years, along with the overall time period to a lesser degree, are characterized by having a level of predictability. The ENSO skill scores are similar to the overall seasonal scores, with NRL1 showing scores close to zero in southern and eastern areas while the other three models show the same values in eastern areas only. Scores in the northwestern region of the domain decreased in all four models compared to Figure 11. The higher scores in the southern and eastern areas of each model run show that the model precipitation is more similar to the observations in these locations than other locations. These results confirm the findings of the temporal correlations shown above.

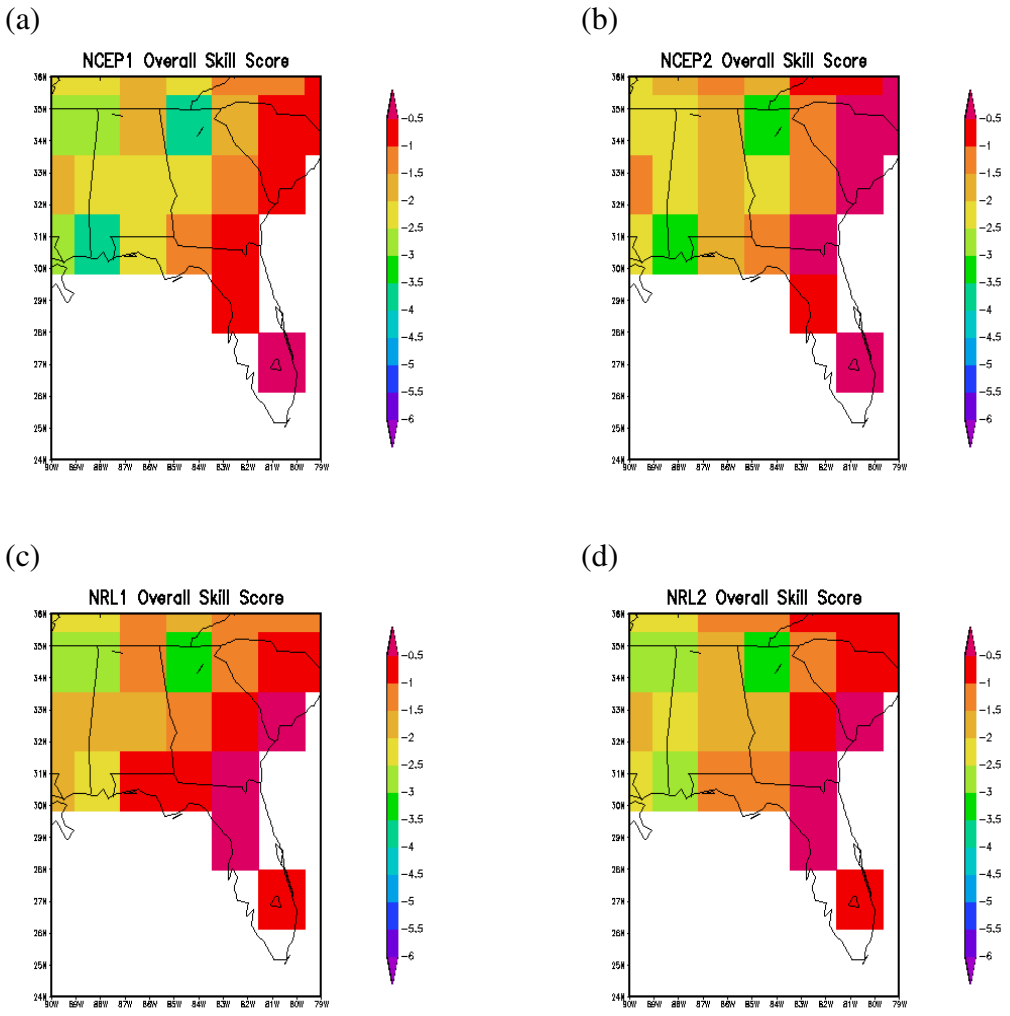

Figure 11: Skill score for each model over all 49 DJF seasons.

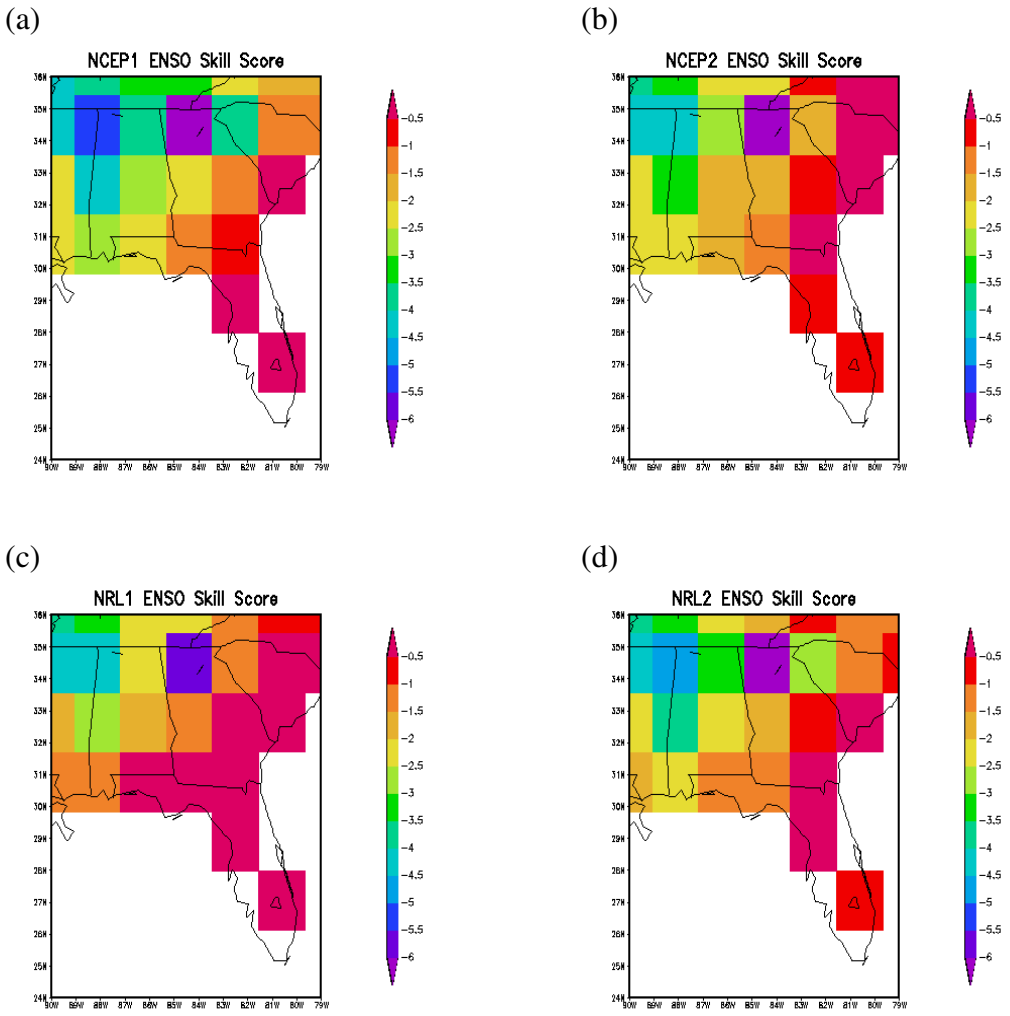

Figure 12: Same as Figure 11, but for the ENSO signal only.

CHAPTER 4

DISCUSSION

The atmospheric response lags tropical Pacific SST forcing by about one to three months (Kumar and Hoerling 2003). A lag correlation of SSTs to model precipitation will either confirm or deny this response. Area-averaged precipitation over the Southeast is correlated to JMA box-averaged SSTs over a series of different lags. Figure 13 shows the observational lag correlation (red) and the four model lag correlations. The observational lag correlation shows a steady increase in value from zero to three months (lags) before decreasing. Both NRL runs show a similar pattern to the observations except for an increase in the three-month correlation value. The NCEP runs show the highest correlation values at zero-months lag with a steady decrease through six months. This shows that the NCEP model runs are more instantaneous in their atmospheric response to tropical Pacific SSTs than the NRL runs, which are similar to the observational pattern.

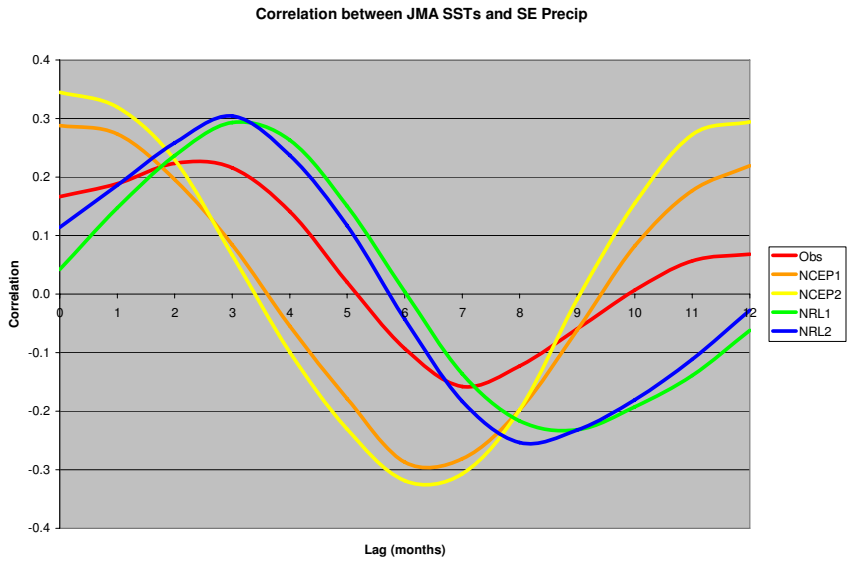

Figure 13: Lag correlation between JMA box-averaged SSTs and area-averaged precipitation over the Southeast.

Since the lag correlation shows a one- to three-month lag of the atmosphere, the correlation of tropical Pacific SSTs to Southeast precipitation patterns must be adjusted accordingly. Figure 14 shows the correlation of DJF precipitation to the area-averaged SST during October, November, and December (OND) over the JMA box. An average of SSTs during OND is used in reference to the JMA index, where OND SST anomalies must be included in the calculation of the index. The observational pattern restricts the highest correlation values to eastern and southern areas of the domain. NCEP2 and NRL1 have the highest correlation values of the four models, with NRL1's highest values located in southern areas and NCEP2's highest values located in eastern areas. NCEP1 shows a similar pattern to the observations, but with lower correlation values in southern and eastern locations. NRL2 has a similar pattern to the observations and NCEP1 but correlation values are higher than NCEP1 particularly over Florida and Georgia (greater than 0.4 for NRL2, about 0.3 on average for NCEP1).

Teleconnection correlations for the ENSO signal are presented in Figure 15. These correlations illustrate the ability of the model to connect warm/cold SSTs to Southeast precipitation patterns during an ENSO event. The observational pattern shows an increase in correlation values in comparison to the seasonal signal in central locations. The highest correlation values are still located in southern and eastern areas. All four models show correlation values of 0.4 or greater along portions of the Gulf and Atlantic coasts. NCEP2 and NRL1 show correlation values greater than 0.4 over the majority of the Southeast. Correlations are high over eastern and south central locations in NRL2 but decrease in northern and western locations, similar to the observational pattern. NCEP1 shows correlation values of at least 0.3 over northern Florida and southern South Carolina, but the pattern is not as distinct as the similar-looking NRL2. The most notable difference between the NCEP runs and the NRL runs is the low correlation over south Florida in NCEP when compared to NRL.

Correlations between the Southeast precipitation and tropical Pacific SSTs for the neutral phase are presented in Figure 16. The observational correlation pattern shows values close to zero (± 0.1) over the majority of the Southeast, with more positive correlations over Florida and portions of South Carolina. Three out of the four model runs show some degree of positive correlation over Florida, with NCEP2 being the outlier. Correlation values are also inconsistent between the models. The NRL runs show moderate to high correlation values over Florida (approximately 0.35) while NCEP1 shows moderate correlations (about 0.3) and NCEP2 shows

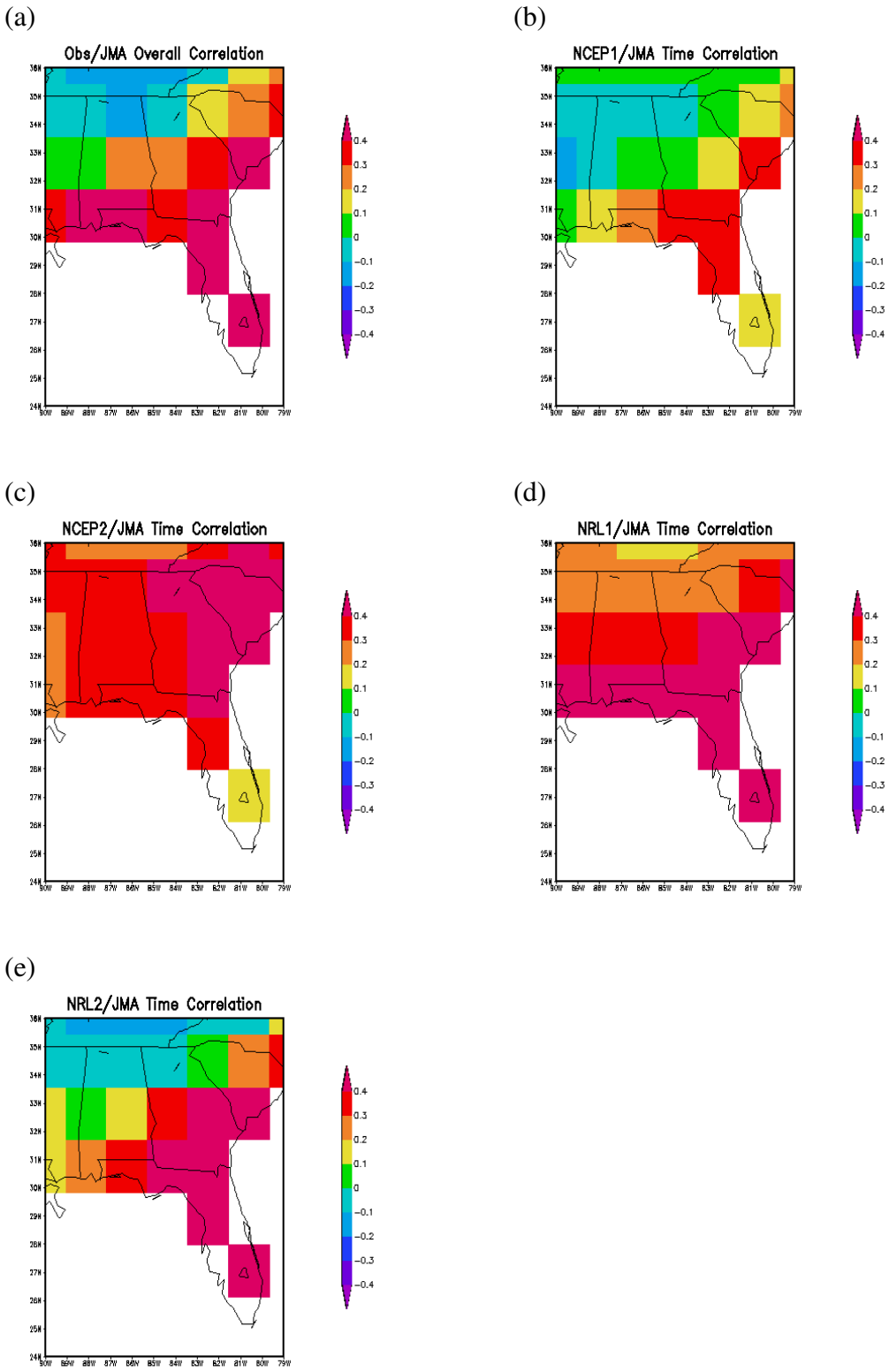

Figure 14: Temporal correlations of JMA box-averaged SSTs and precipitation for a) the observations and b-e) the four model runs.

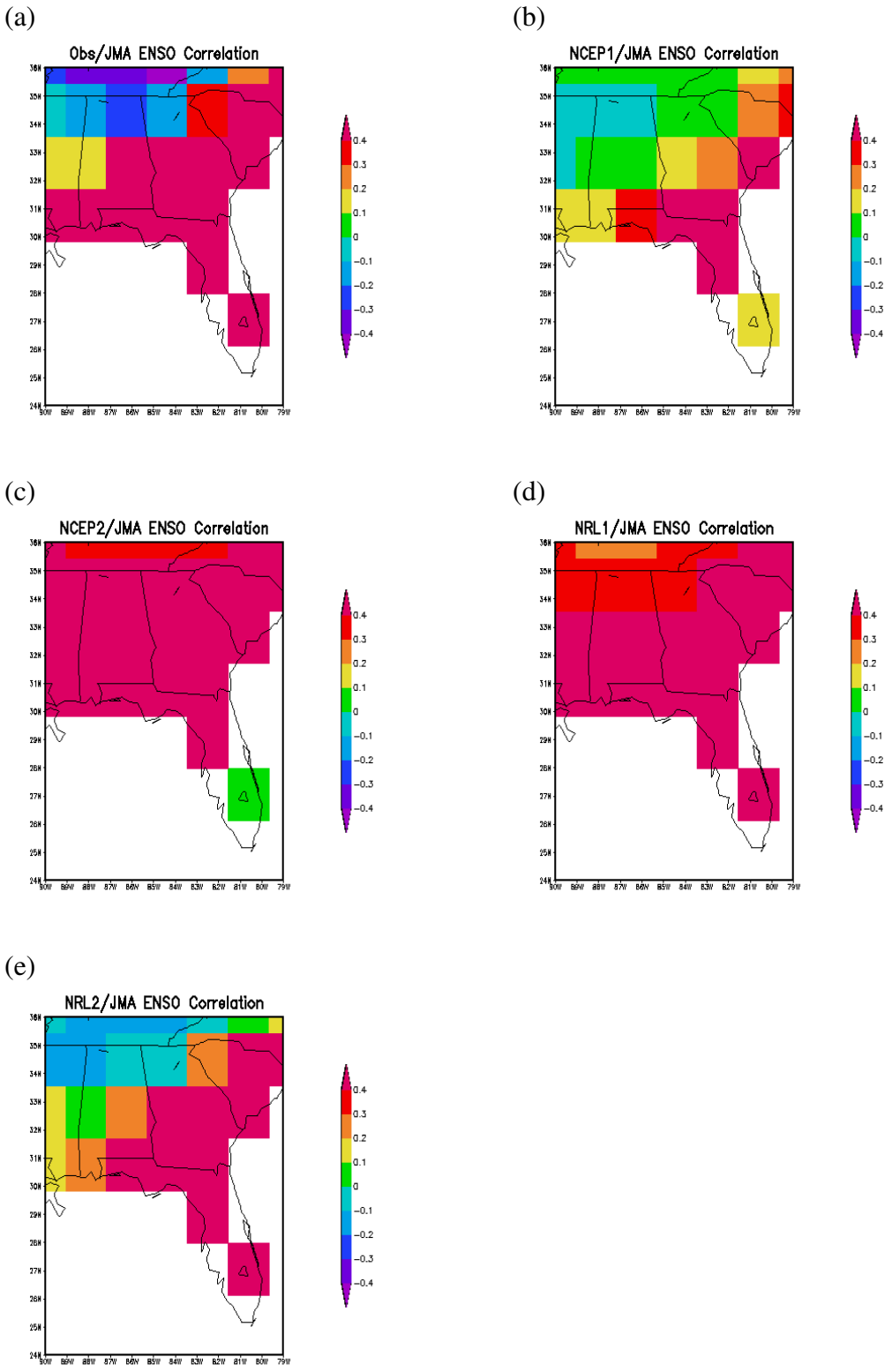

Figure 15: Same as Figure 14, but for the overall ENSO signal.

low correlations (about 0.1) over the same area. The lack of consistently high correlation values over the domain is due to the inherent variability of the neutral phase. In NCEP1, large negative correlation values appear over the area where the bias is the largest (northwestern locations). NCEP2 and NRL2 show more positive correlation values than NCEP1 and NRL1, which could indicate a similarity in the jet stream patterns for each pair of models.

In general, the model/observation correlations have lower values than the SST/precipitation correlations. The commonality between the two sets of correlations is that the highest values with respect to each individual plot appear in southern and eastern areas. Combining the correlations from Figure 5 with those of Figure 14, the model appears to have some skill in predicting precipitation over the Southeast, especially in areas where the highest correlations appear consistently. The same result holds true for the ENSO signal model/observation correlations in Figure 6 and the SST/precipitation correlations in Figure 15.

The correlation values and resulting patterns are affected by position of the subtropical jet stream in each of the model runs. Figure 17 shows the 200-mb wind speed and direction over the eastern Pacific and North America for the NCEP reanalysis (observations) and each model run. The observations show a jet max located along an axis from Louisiana to Bermuda. The core of the jet max is located over the Carolinas. The path of the jet stream is a southern route over parts of the tropical Pacific and Mexico before traveling over the Southeast. NCEP1 and NRL2 show a southward shift of the jet stream compared to NCEP2 and NRL1. The NRL1 correlation pattern is shifted somewhat northward of NCEP1 and NRL2, which indicates that the jet stream is also shifted northward. The jet max located over the western Atlantic is shifted slightly northward in NRL1 compared to the other models, which is enough to make a difference in the correlation pattern. However, the alignment of the jet stream over the Southeast in NRL1 is similar to NCEP1 and NRL2 due to the similarity of the correlation patterns spatially. NCEP2 shows a different spatial pattern than the other three models. This particular pattern would indicate that the northward bend of the jet stream occurs further west than the other three models. However, it appears as though the wind speed has more influence on the spatial pattern of the correlations than the wind direction since there is very little difference in the flow, especially over the Southeast. When compared to the observations, all four models show the jet stream shifted north over the Pacific. The obvious difference is the strength of the jet max over the Southeast, with the models over-estimating the wind speed by as much as 10 m/s.

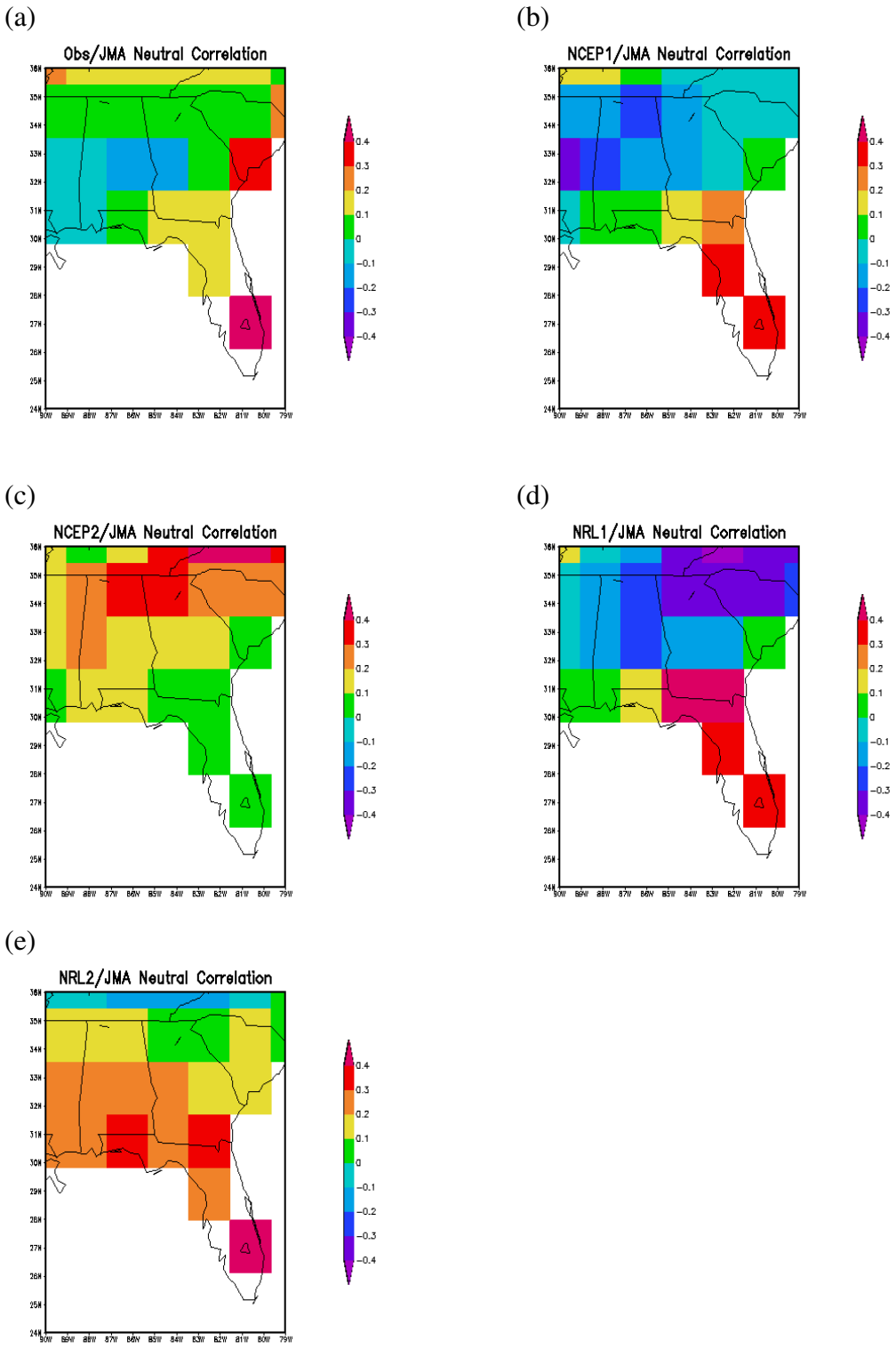

Figure 16: Same as Figure 14, but for neutral.

(a)

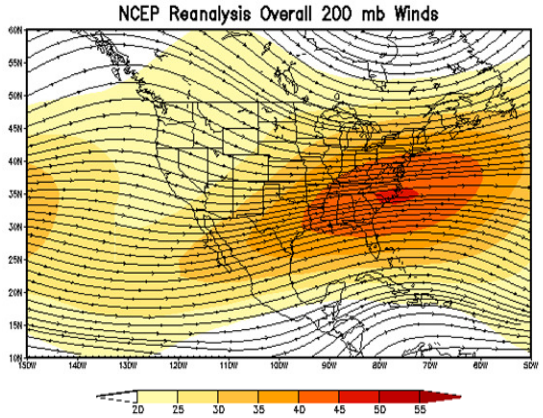

(b)

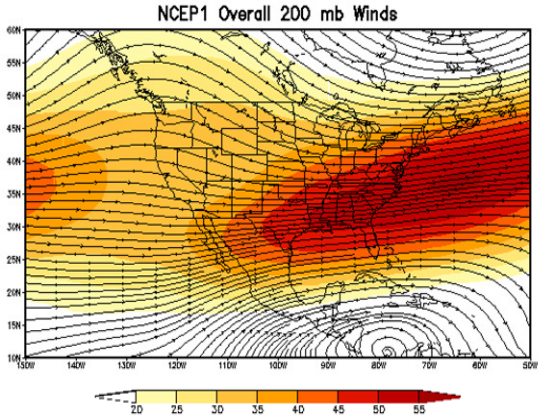

(c)

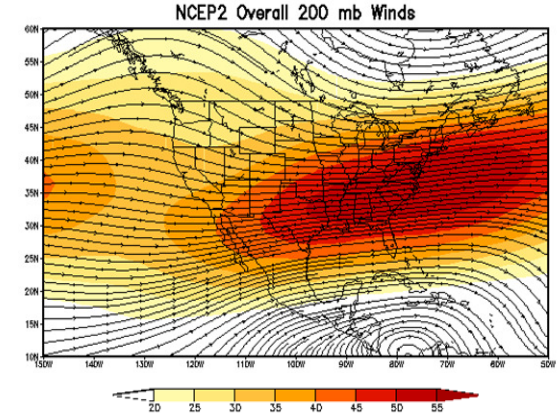

(d)

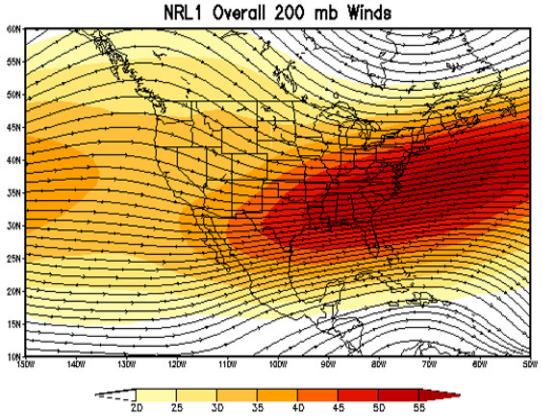

(e)

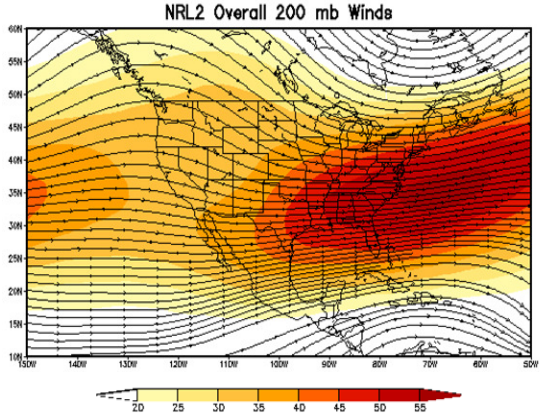

Figure 17: Winter seasonal averaged 200-mb wind speed (shaded) and direction (streamlines) for a) NCEP reanalysis and b-e) each of the four models. Wind speed is in m/s.

The strength of the jet stream determines how much moisture is transported via storm systems to the Southeast. A weaker jet stream means less moisture is acquired from the tropical Pacific and thus transported to the Southeast. A stronger jet stream is more able to carry the moisture over the long distances between the tropical Pacific and the Southeast. The correlation values in Figure 14 can be used as an indicator of the strength of the jet stream. Higher correlation values signify a jet stream that is strong enough to transport moisture from the tropical Pacific to the Southeast. NCEP1 has a weaker jet stream than the similarly-patterned NRL2, which is evident in the lower correlation values over the coastal areas. The jet stream max is approximately 5 m/s lower in NCEP1 than the other three models. The other three models show correlation values that indicate a strong jet stream (approximately 0.4 or greater). The over-estimation of the wind speed in the jet max appears to have inflated some correlation values, especially in NCEP2 and NRL1. The observation SST/precipitation correlations combined with the NCEP reanalysis winds illustrate that jet max wind speeds do not need to be as high as the model winds to establish a connection between the Southeast and the tropical Pacific.

The position of the jet stream over the Southeast, which steers synoptic weather systems, changes with each ENSO phase. During El Niño, the jet stream shifts south over the warm waters of the tropical eastern Pacific and eventually moves over the Gulf of Mexico. This allows for the moisture over the tropical eastern Pacific to reach the Southeast. During La Niña, the jet stream is more amplified over the western U.S. due to the shift in the warm pool westward over the tropical Pacific and thus takes a more northern track over the Southeast, shifting the maximum precipitation northward. The lack of consistency in the model/observation correlations and SST/precipitation correlations between the models and the two correlation types underlies larger problems that have yet to be identified.

In order to assess the difference between the El Niño and La Niña jet stream positions, the La Niña wind speed and direction was subtracted from the El Niño wind speed and direction. This allows for a more direct comparison of the difference between El Niño and La Niña jet stream patterns. Figure 18 shows the 200-mb wind difference between the warm and cold phases for the NCEP reanalysis winds (observations) and the four model runs. The warmer (cooler) colors indicate locations where El Niño winds are stronger (weaker) than La Niña winds. The observations show the El Niño jet stream to be located over southern North America. The jet

(a)

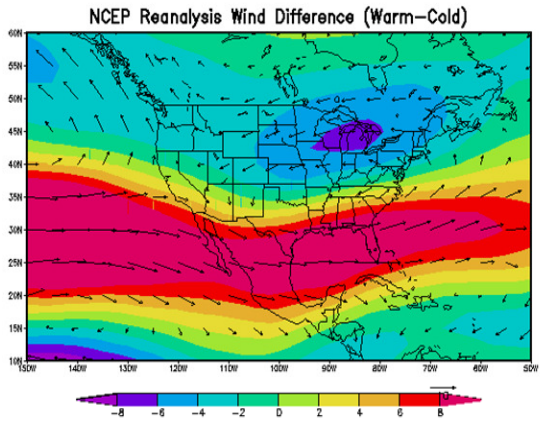

(b)

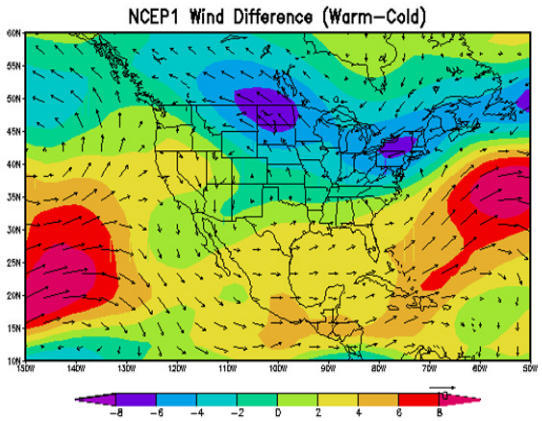

(c)

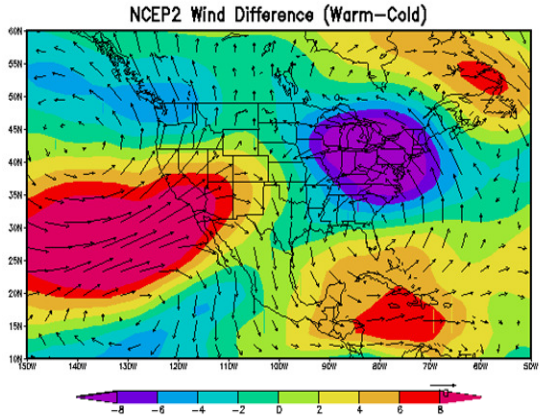

(d)

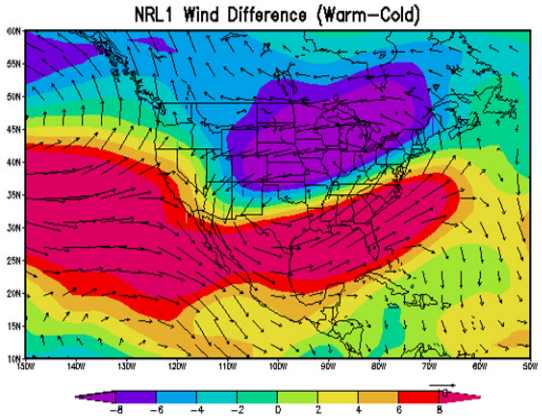

(e)

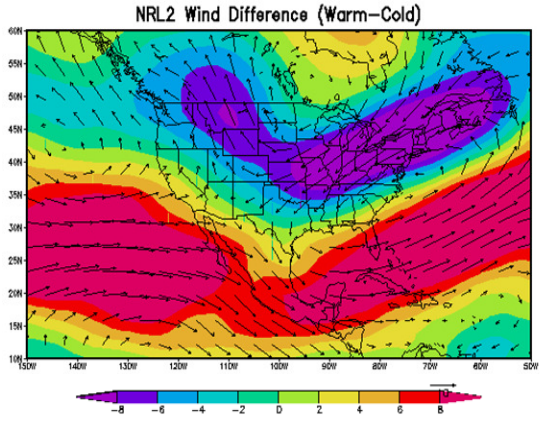

Figure 18: Difference between DJF El Niño (warm) and La Niña (cold) 200-mb winds for a) NCEP Reanalysis and b-e) the four model runs. Units in m/s.

stream shifts its position northward over the North Pacific and over the midwestern U.S. during La Niña. Both NCEP runs show an area of disconnection in the southern El Niño jet stream location. The NCEP1 La Niña jet stream location is similar to the observations, while NCEP2 shows the La Niña jet streak shifted south of the observations. Both NRL runs show similar patterns for the El Niño jet stream. The only difference between the NRL runs and the observations is the strength of the La Niña jet stream, with the NRL runs showing higher wind speeds than the observations. The results of these model wind differences show that the NRL convection scheme is more able than the NCEP scheme to reproduce ENSO wind patterns, which affects the resulting precipitation over the Southeast.

The 200-mb winds are not the only atmospheric variable that affects the ENSO precipitation patterns over the Southeast. The 500-mb height patterns can also affect the resulting precipitation patterns, but to a lesser degree than the upper-level winds. This is achieved through the PNA pattern, which can be influence by ENSO as well as other atmospheric phenomena. Since the upper-level wind patterns are stable during an ENSO event, the PNA pattern sets up in a phase-specific method, where El Niño can result in a positive PNA pattern and La Niña can result in a negative PNA pattern. A positive PNA pattern occurs when height anomalies are negative over the eastern Pacific, positive over western areas of North America, and negative over eastern North America. This forms a trough-ridge-trough pattern from west to east which helps to enhance the El Niño teleconnection and resulting signatures over the Southeast. Figure 24 shows the 500-mb height anomalies over the PNA region for El Niño. The trough-ridge-trough pattern is seen in the NCEP reanalysis (observations) and all four models. The difference is the placement and value of the respective anomalies, which can cause differences in the resulting correlation patterns. The observations show an area of negative anomalies with a minimum value of -30 m over the Southeast. NCEP2 and NRL1 show two distinct areas of negative anomalies and one clear area of positive anomalies between the negative areas. This creates a clear trough-ridge-trough pattern. However, the negative anomalies over the Southeast are larger in NRL1 than NCEP2, with NRL1 over-estimating the anomalies by 30 m over the observations. NRL2 shows a smaller area of negative anomalies over the Pacific which extends through to the Southeast. The positive anomalies are similar in strength and location to NRL1. However, it is the pattern of the negative anomalies that would affect the mid-level flow. NCEP1 has a similar problem to NRL2 with the negative anomalies.

(a)

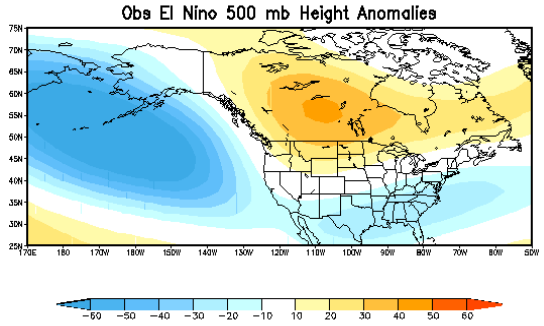

(b)

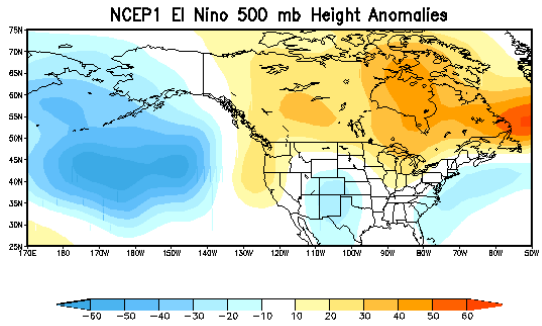

(c)

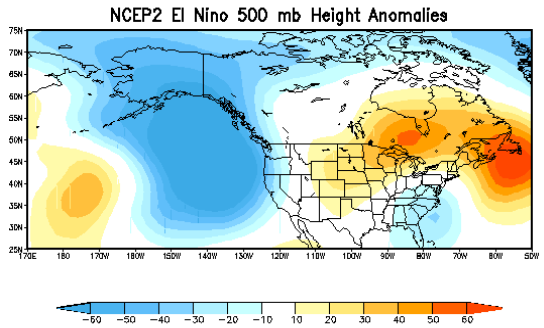

(d)

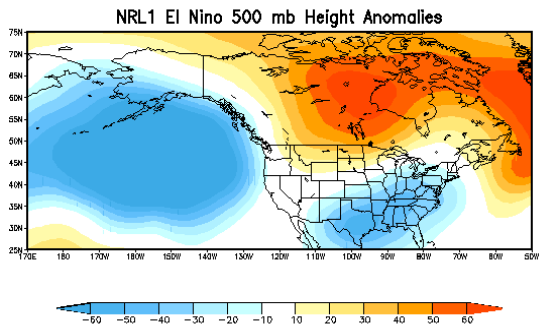

(e)

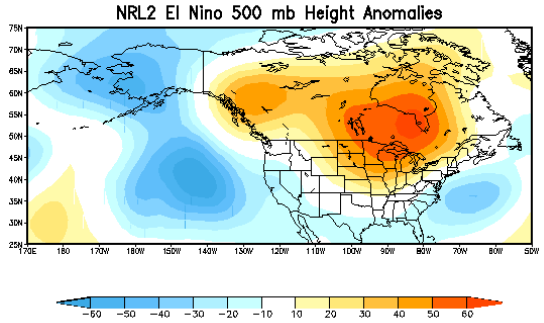

Figure 19: El Niño 500-mb height anomalies over the PNA region. Units in m.

The eastern area of negative anomalies is split into two parts, which also affects the mid-level flow in the same manner as NRL2. Also, the positive anomalies are not as large as the other models, thus affecting the mid-level flow to a greater extent. The important finding is that the model height anomaly fields are generally similar to the observational field, with the exception of magnitude problems over certain regions. As long as the model can capture the general large

scale problems, smaller-scale regional patterns such as Southeast precipitation will be captured by the model.

The negative PNA pattern, associated with La Niña, is generally the opposite of the positive pattern. The pattern manifests itself with positive height anomalies over the eastern Pacific and eastern North America, and negative anomalies over western North America, thereby forming a ridge-trough-ridge pattern. Figure 25 shows the La Niña 500-mb height anomalies

(a)

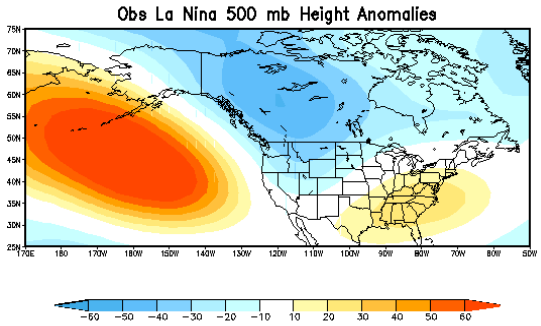

(b)

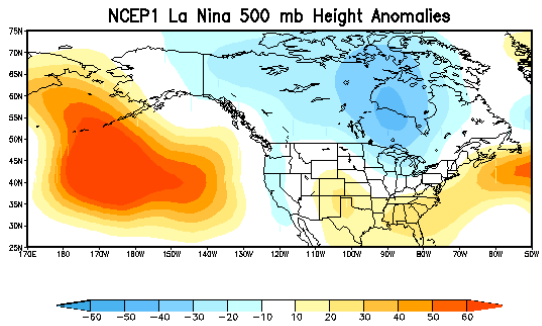

(c)

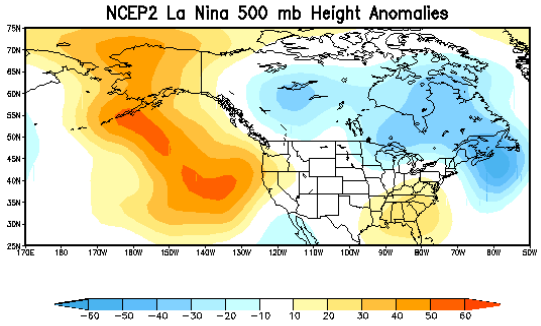

(d)

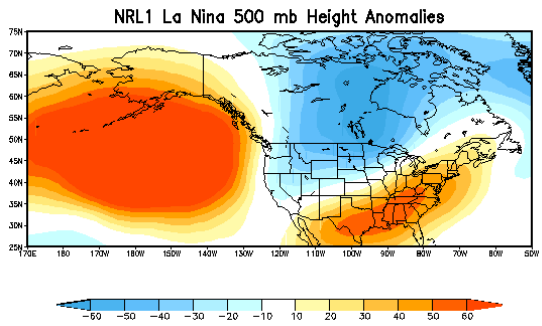

(e)

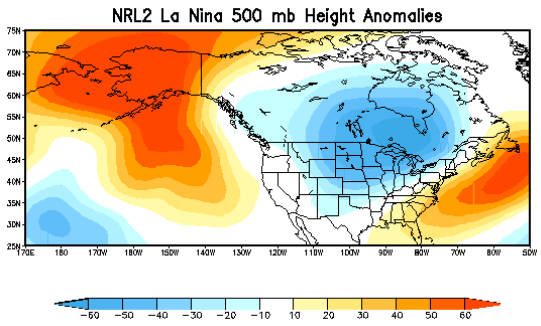

Figure 20: Same as Figure 19, but for La Niña.

over the PNA region. Since the anomaly pattern is opposite of the El Niño pattern, the opposite precipitation signature should form for La Niña. The observations in La Niña appear similar in magnitude to the El Niño observations, with the Southeast positive anomalies having a value of 30 m or less. NRL1 shows the ridge extending from northern Mexico to the Northeast U.S. while the other three models show the ridge starting in the Southeast and extending through the Northeast and into the Atlantic. The westward shift of the ridge by NRL1 affects the mid-level flow, thereby adjusting the storm track and changing the precipitation amounts over the Southeast. It appears as though there only needs to be an area of negative anomalies over the western/central U.S. to create the trough and adjust the mid-level flow over the eastern U.S. Again, the models over-estimate the magnitude of the height anomalies, especially the Southeast positive anomaly in NRL1. However, all four models captured the general negative PNA pattern which allows the model to then capture regional-scale phenomena.

CHAPTER 5

CONCLUSIONS

The Southeast U.S. is known to have a clear teleconnection to tropical Pacific SSTs. More specifically, precipitation tends to be very sensitive to changes in SSTs during the winter season, resulting in different patterns for each ENSO phase. Models can be used to test predictions against observations due to the predictability of the region. Ensemble data from the FSUGSM using the NRL and NCEP convection schemes were used to study winter precipitation patterns over the Southeast from 1950-1999. The two different convection schemes generated precipitation through different cumulus cloud parameterizations. Model precipitation data from four model runs were then compared to observations using multiple techniques to assess the similarity of the two datasets. Wind and height data were also used to assess the large-scale patterns that affect the Southeast.

The large variability of the ensemble was evident in both climatology and ENSO signal. The NRL convection scheme runs produced ENSO anomaly patterns that were closer to the observations than the NCEP convection scheme runs. The resulting values from both sets of temporal correlations (model/observations and SST/precipitation) were dependent on the model run. A possible dependence on initial conditions appears within each convection scheme. This dependence manifests itself in two ways through the statistical calculations. Overall, the model runs were too dry over the Southeast.

The variance of each model run was less than the observational variance, which may have been affected by the dry bias in the model. The skill scores confirm the correlation patterns that develop in both the seasonal signal and the ENSO signal. Areas that were closest to the observations in the skill scores appear as areas with the highest correlation values. The lag correlation showed a one- to three-month lag between tropical Pacific SSTs and Southeast precipitation for both NRL runs, while a zero- to one-month lag appeared in the NCEP runs.

This discrepancy in the lag correlations of the convection schemes may explain the difficulty of the NCEP scheme to represent the ENSO signal over the Southeast relative to the NRL scheme.

Differences in winds and heights between the model runs affected the teleconnection between the tropical Pacific and the Southeast. The 200-mb wind patterns showed a dependence on convection scheme. The NRL runs were more similar to the observations, which influenced the connection between the tropical Pacific and the Southeast. The wind patterns at 850-mb (not shown) were found to have very little difference between phases and therefore, have little effect on the correlations due to the lack of pattern change between phases. The 500-mb height anomaly patterns over the PNA region for each model run showed similar patterns to the observations and what has been found previously (Leathers and Palecki 1992). The placement of the anomalies differed in each model, affecting the mid-level flow and the resulting precipitation patterns.

Precipitation modeling is far from being perfect. However, much has been done over the years to improve precipitation simulations. The goal of this research was to be able to examine the similarity of ENSO precipitation patterns over the Southeast to observational patterns. The model runs produced precipitation amounts that were too dry overall. The small ensemble size limited the reliability of the ensemble. With only 4 members, the ensemble may have been skewed by an outlying member in certain ENSO phases (e.g. NCEP1 precipitation anomalies in El Niño and NCEP2 precipitation anomalies in La Niña). Future work includes verification of the correlations using a statistical test to show significance (Kolmogorov-Smirnov test). This analysis may also be extended to other areas of the world showing a precipitation signal related to ENSO. The analysis can also be applied to other seasons over the same ENSO-sensitive areas. The addition of another convection scheme or an increase in ensemble size using the current convection schemes in the FSUGSM will address the reliability issue of the ensemble, which may eventually be able to produce more reliable forecasts than the individual model runs. Additionally, the model and data will be transferred to the International Research Institute (IRI) for Climate and Society as part of the multi-model experiment.

REFERENCES

Cocke, S., and T. E. LaRow, 2000: Seasonal Predictions Using a Regional Spectral Model Embedded within a Coupled Ocean-Atmosphere Model. *Mon. Wea. Rev.* **128,** 689-708.

—, —, and D. W. Shin, 2006: Seasonal Rainfall Predictions over the Southeast U.S. using the FSU Nested Regional Spectral Model. *J. Appl. Meteor.,*(in review).

Deser, C., A. S. Phillips, and J. W. Hurrell, 2004: Pacific Interdecadal Climate Variability: Linkages between the Tropics and the North Pacific during Boreal Winter since 1900. *J. Climate,* **17,** 3109-3124

Hoerling, M. P., and A. Kumar, 2002: Atmospheric Response Patterns Associated with Tropical Forcing. *J. Climate,* **15,** 2184-2203.

Horel, J. D., and J. M. Wallace, 1981: Planetary-Scale Atmospheric Phenomena Associated with the Southern Oscillation. *Mon. Wea. Rev.,* **109,** 813-829.

Japan Meteorological Agency (JMA), Marine Department, 1991: Climate Charts of Sea Surface Temperatures of the Western North Pacific and the Global Ocean. 51 pp.

Kao, C.-Y. J., A. Quintanar, M. J. Newman, W. Eichinger, D. L. Langley, and S.-C. Chen, 1996: Climate Simulations with NCAR CCM2 Forced by Global Sea Surface Temperature, 1950-89. *J. Climate,* **9,** 3530-3547.

Kumar, A., and M. P. Hoerling, 2003: The Nature and Causes for the Delayed Atmospheric Response to El Niño. *J. Climate,* **16,** 1391-1403.

LaRow, T. E., and T. N. Krishnamurti, 1998: Initial Conditions and ENSO predictions using a coupled ocean-atmosphere model. *Tellus*, **50A,** 76-94.

Lau, K. M., and J. S. Boyle, 1987: Tropical and Extratropical Forcing of the Large-Scale Circulation: A Diagnostic Study. *Mon. Wea. Rev.,* **115,** 400-428.

Leathers, D. J., B. Yarnal, and M. A. Palecki, 1991: The Pacific/North American Teleconnection Pattern and United States Climate. Part I: Regional Temperature and Precipitation Associations. *J. Climate,* **4,** 517-528.

—, and M. A. Palecki, 1992: The Pacific/North American Teleconnection Pattern and United States Climate. Part II: Temporal Characteristics and Index Specifications. *J. Climate,* **5,** 707-716.

Livezey, R. E., M. Masutani, A. Leetmaa, H. Rui, M. Ji, and A. Kumar, 1997: Teleconnective Response of the Pacific-North American Region Atmosphere to Large Central Equatorial Pacific SST Anomalies. *J. Climate,* **10,** 1787-1820.

Palmer, T. N., and Coauthors, 2004: Development of a European Multimodel Ensemble System for Seasonal-to-Interannual Prediction (DEMETER). *Bull. Amer. Meteor. Soc.,* **85,** 853-872.

Quan, X. W., P. J. Webster, A. M. Moore, and H. R. Chang, 2004: Seasonality in SST-Forced Atmospheric Short-Term Climate Predictability. *J. Climate,* **17,** 3090-3108.

Reynolds, R. W., and T. M. Smith, 1995: A High-Resolution Global Sea Surface Temperature Climatology. *J. Climate,* **8,** 1571-1583.

Ropelewski, C. F., and M. S. Halpert, 1986: North American Precipitation and Temperature Patterns Associated with the El Niño/Southern Oscillation (ENSO). *Mon. Wea. Rev.,* **114,** 2352-2362.

—, and —, 1987: Global and Regional Scale Precipitation Patterns Associated with the El Niño/Southern Oscillation. *Mon. Wea. Rev.,* **115,** 1606-1626.

Shin, D. W., S. Cocke, T. E. LaRow, and J. J. O'Brien, 2005: Seasonal Surface Air Temperature and Precipitation in the FSU Climate Model Coupled to the CLM2. *J. Climate,* **18,** 3217-3228.

Walker, G. T., 1924: Correlation in seasonal variations of weather, IX: A further study of world weather. *Mem. Indian Meteor. Soc.,* **24,** 275-332.

—, and E. W. Bliss, 1932: World Weather V. *Mem. Roy. Meteor. Soc.,* **4,** 53-84.

Willmott, C. J., and K. Matsuura, cited 2005: Terrestrial Air Temperature and Precipitation. [Available online at http://climate.geog.udel.edu/~climate.]

Yarnal, B., and H. F. Diaz, 1986: Relationships between extremes of the Southern Oscillation and the winter climate of the Anglo-American Pacific coast. *J. Climatol.,* **6,** 197-219.

BIOGRAPHICAL SKETCH

I was born in Pittsburgh, Pennsylvania on October 23, 1981. I spent only three and a half years there before moving to a small village called Landenberg in southeastern Pennsylvania. After 6 years there, I then moved again, this time to the Lehigh Valley (more like the foothills of the Pocono Mountains) and have been there ever since. Even though I've spent most of my life living in eastern Pennsylvania, I still feel like the Pittsburgh area is home because of all the family members still there.

I graduated from Northampton Area Senior High School in 1999 as a member of the National Honor Society. I knew long before graduation that I wanted to study meteorology in college, which left the college decision much easier to make. I attended the Pennsylvania State University and graduated with my B.S. in meteorology in 2003.

Even though weather is my chosen profession, my ultimate passion is horseback riding. I've been riding horses since 1992, but the horse thing has been in me since I was little. My chosen discipline now is dressage, after riding hunters and jumpers for about 7 years. I have two horses, a 24-year-old Quarter Horse and a 5-year-old Friesian/Appaloosa cross. The 24-year-old is my first horse, with the 5-year-old being my new project after finishing up my M.S. My goal is to reach the Grand Prix level (highest level) with the young one, as long as he is up for the task.